TECHNICAL REPORT RL-80-7

FLAW DETECTION AND EVALUATION OF COMPOSITE CYLINDERS USING LASER SPECKLE INTERFEROMETRY AND HOLOGRAPHY

Terry L. Vandiver
Ground Equipment and Missile Structures Directorate
US Army Missile Laboratory

23 November 1979

U.S. ARMY MISSILE COMMAND
Redstone Arsenal, Alabama 35809

DISPOSITION INSTRUCTIONS

DESTROY THIS REPORT WHEN IT IS NO LONGER NEEDED. DO NOT RETURN IT TO THE ORIGINATOR.

DISCLAIMER

THE FINDINGS IN THIS REPORT ARE NOT TO BE CONSTRUED AS AN OFFICIAL DEPARTMENT OF THE ARMY POSITION UNLESS SO DESIGNATED BY OTHER AUTHORIZED DOCUMENTS.

TRADE NAMES

USE OF TRADE NAMES OR MANUFACTURERS IN THIS REPORT DOES NOT CONSTITUTE AN OFFICIAL ENDORSEMENT OR APPROVAL OF THE USE OF SUCH COMMERCIAL HARDWARE OR SOFTWARE.

UNCLASSIFIED

SECURITY CLASSIFICATION OF THIS PAGE *(When Data Entered)*

REPORT DOCUMENTATION PAGE		READ INSTRUCTIONS BEFORE COMPLETING FORM
1. REPORT NUMBER RL-80-7	2. GOVT ACCESSION NO.	3. RECIPIENT'S CATALOG NUMBER
4. TITLE *(and Subtitle)* FLAW DETECTION AND EVALUATION OF COMPOSITE CYLINDERS USING LASER SPECKLE INTERFEROMETRY AND HOLOGRAPHY		5. TYPE OF REPORT & PERIOD COVERED Technical Report 6. PERFORMING ORG. REPORT NUMBER
7. AUTHOR(s) Terry L. Vandiver		8. CONTRACT OR GRANT NUMBER(s)
9. PERFORMING ORGANIZATION NAME AND ADDRESS Commander US Army Missile Command ATTN: DRSMI-RLA Redstone Arsenal, Alabama 35809		10. PROGRAM ELEMENT, PROJECT, TASK AREA & WORK UNIT NUMBERS
11. CONTROLLING OFFICE NAME AND ADDRESS Commander US Army Missile Command ATTN: DRSMI-RPT Redstone Arsenal, Alabama 35809		12. REPORT DATE 23 November 1979 13. NUMBER OF PAGES 88
14. MONITORING AGENCY NAME & ADDRESS*(if different from Controlling Office)*		15. SECURITY CLASS. *(of this report)* Unclassified 15a. DECLASSIFICATION/DOWNGRADING SCHEDULE NA

16. DISTRIBUTION STATEMENT *(of this Report)*

Distribution approved for public release; distribution unlimited.

17. DISTRIBUTION STATEMENT *(of the abstract entered in Block 20, if different from Report)*

18. SUPPLEMENTARY NOTES

19. KEY WORDS *(Continue on reverse side if necessary and identify by block number)*

Speckle Interferometry
Nondestructive Testing
Flaw Detection
Young's Fringes
Displacement Analysis
Composite Material Testing
Holography

20. ABSTRACT *(Continue on reverse side if necessary and identify by block number)*

The objective of this work was to determine what constitutes a flaw in a composite tube. Speckle interferometry and holography were used to measure surface displacements of 108 fiber reinforced thin wall cylinders. E-glass, S-glass and Kevlar fibers were used. Cut fiber and impact flaws were investigated. A new automated laser speckle interferometry displacement contour analyzer was used in conjunction with a computer for data analysis. The system analyzes 5000 data points in less than four minutes. Full field reconstruction

(over)

DD FORM 1 JAN 73 1473 EDITION OF 1 NOV 65 IS OBSOLETE

UNCLASSIFIED

SECURITY CLASSIFICATION OF THIS PAGE *(When Data Entered)*

of laser speckle interferograms and holograms is presented. The techniques described give the investigator a full field displacement picture of the flawed structures as well as displacement data that can be used to determine stresses and strains.

ACKNOWLEDGMENTS

The author hereby expresses his appreciation to Mr. J. A. Schaeffel Jr. for his guidance on interferometry and the computer aided reduction system; Mr. Keith O. Rogers, Mr. R. B. McGowan, and Ms. A. F. Dempsey for their assistance with the laboratory work and data reduction.

CONTENTS

ILLUSTRATIONS

Figure Page

ILLUSTRATIONS (Continued)

Figure Page

ILLUSTRATIONS (Concluded)

Figure — Page

I. INTRODUCTION

An increasing demand for new materials has prompted the use of composites for such applications as rocket launch tubes,motor cases, and aircraft tail sections. Filament-wrapped composite structures have merit because of the high strength to weight ratio and low cost of manufacture. With the increasing use of composites for structural applications there exists greater needs for flaw detection and evaluation. Because of the nonhomogeneity of composite structures, different techniques of flaw detection must be used. The purpose of this work was to determine what constitutes a valid flaw in a composite tube.

The types of flaws observed were cut fiber in the cylinder tube wall and dynamic impact flaws. The cut fiber flaws are likely to develop in a manufacturing process during winding whereas the impact flaws would most likely occur in the structure after manufacture. Most of the work was devoted to impact flaws because flaws of this type are the most likely to occur in nature.

Speckle interferometry and holography were the optical techniques selected to determine what constituted a flaw. These techniques depend on the fringe patterns developed from double exposure photography of the laser speckle pattern between a deformed and undeformed structure. The techniques are nondestructive and produce extremely accurate displacement data.

The greatest advantage of using speckle interferometry and holography is that the investigator has a full field 'hands off' view of the deformable body. One can easily determine stresses and strains from the displacement data [1].

Section II discusses the type of composite materials used and preparation of the test cylinders while Section III describes the type flaws and the techniques used to introduce them. Section IV describes the optical test setups and procedures used for speckle interferometry and holography while Section V describes the techniques used to analyze the data. Appendix A contains photographs of full field reconstructed speckle interferograms and Appendix B contains photographs of full field reconstructed holograms.

II. MATERIAL CONSIDERATIONS

A. Composite Material Selection and Manufacture

One hundred eight fiber reinforced composite cylinders were manufactured to be used in developing nondestructive experimental techniques to detect and evaluate flaws. The composite cylinders were fabricated by a filament winding process where a continuous bundle of fibers is wetted with epoxy and wound onto a cylindrical mandrel. Three groups of thirty six structures per group were prepared. Each group consisted of three subgroups having helical wrap angles of either ±45 degree, ±60 degree, or ±70 degree.

Each group of 36 structures was made from a different type fiber:

Group 1-
- E-glass
- Type 801 AB
- G Filament
- Yield 1167 yard/pound
- Owens Corning Fiberglass Co.

Group 2-
- S-glass
- Type S-1014
- 12 End Roving, 204 Filaments Per End
- S-24 Finish
- Ferro Corporation

Group 3-
- Kevlar 49
- Aramid Fiber

- 4560 Denier
- Type 969 Aerospace Roving

The resin system for all three groups consisted of:

- EPON 828 100 Parts By Weight
- NMA Hardener 90 Parts By Weight
- BDMA Accelerator 1 Part by Weight

Oven cure time for the cylinders was 8 hours at 200 degree F and 16 hours at 400 degree F.

B. Test Specimen Preparation

The fiber reinforced composite cylinders were received in approximately 36-inch lengths. Three 10-inch long test specimens were cut from each cylinder. The extreme ends of the 36 inch long tubes were avoided because of the nonuniformity of cylinder wall thickness. An 8-inch region on each test specimen was painted with flat white paint to provide a good illumination surface required for speckle interferometry.

Each specimen received 2 rotation markers 180 degrees apart located at the bottom of the test cylinders and a nomenclature code located at the top. *Figure1* shows a typical test specimen prepared for loading and speckle interferometry. One of the 180 degree markers is axially aligned with the test flaw to determine the orientation of the flaw with respect to the cylinder. The test nomenclature code was set up as shown in *Figure 2* using test cylinder Number 1 as an example.The interferogram letter A or B designates at which 180 degree rotation the interferogram is made. The A side of the cylinder is the side which contains the flaw.

III. FLAW TYPES

A. Impact Flaws

Compressive impact flaws were programmed into the outer cylinder walls by the fixture shown in *Figure 3.* The fixture was designed to apply a compressive impact load into the outer cylinder wall by a free fall 76 mm diameter mass dropping a predetermined

height onto a dart which rests on the tube wall. The dart geometries are shown in *Figure 4*. The tube fits snugly onto a steel localizing bar so that the energy will be dissipated over a very small region of the test cylinder, thus eliminating flexure considerations. One can calculate the amount of energy transferred to the cylinder wall by Equation (1):

$$KE = \tfrac{1}{2} MV^2 \tag{1}$$

where M is the free fall mass and V is the terminal velocity of the mass at impact. Different levels of energy were applied to the tube walls by varying the height of the drop mass. Notches equally spaced at 2.5 cm increments allowed the mass to be dropped from a height of 2.5 to 45.7 cm. Different levels of energy can also be obtained by using different drop masses.

B. Cut Fiber Flaws

A flaw that consists of cut fiber damage would most likely occur as a malfunction in a manufacturing operation either from excessive wrap tension or damaged fiber from the manufacture. The flaws were made by cutting an entire roving during the wrapping process. The bundle of fiber strands was then placed directly beside where it was cut, the mandrel manually rotated until the process could be continued automatically.

IV. OPTICAL TEST SETUP AND PROCEDURE

A. Laser Speckle Interferometry Setup

Two interferograms were made of each composite test cylinder, one of the flawed side A and one of the unflawed side B *Figure 1*. The experimental test arrangement for speckle interferometry is shown in *Figure 5*. The loading fixture to hold the test cylinders consisted of two endcaps equipped with rubber O-rings to allow the cylinder to deform unrestricted. The endcaps were held together with a threaded center rod as shown in *Figure 6*. To reassure that no restriction occurred at the top of the cylinder a thin coat of lubricant was applied to the top O-ring and to the interior region of the test cylinder that came in contact with the endcap. A clamp was used to restrain the bottom end of the cylinder.

A double exposure photography technique was used to make the interferogram. A 102 x 127mm glass film plate was double exposed: one exposure was made with the test cylinder loaded and one with the cylinder unloaded. After the cylinders were loaded, they were allowed to stabilize for a minimum of 30 seconds before the first exposure was made. A

remote shutter control and timer was used to allow the test specimen to be illuminated by a Spectra Physics model 166 argon laser adjusted at 0.45 watts. The film plate was exposed for 30 seconds in both the loaded and unloaded conditions thus producing the speckle interferogram. The exposed film plates were then developed using conventional techniques.

B. Holography Test Setup

Holography also utilizes the double exposure technique of the light wave interference from a deformed body. Two holograms were made of the test cylinders so that the flawed side could be compared to the unflawed side. Holography requires an object beam and a reference beam as can be seen in the experimental test arrangement shown in *Figure 7*. The loading conditions were the same as for speckle interferometry that is constraining the bottom of the cylinder while allowing the top to move freely. A much lower load pressure is required in holography. A Spectra Physics model 125 HeNe laser powered at 50 mW was used to generate the light source for the object and reference beams. The film plate was exposed for 28 seconds in both the loaded and unloaded conditions thus producing the hologram. The exposed film plates were developed using the same techniques as for speckle interferometry. The load pressures used for speckle interferometry and holography are shown in *Table 1*.

V. DATA ANALYSIS

A. Speckle Interferometric and Holographic Analysis

When a diffuse surface is illuminated by the coherent radiation from a laser, a grainy speckle effect may be seen on the surface. This effect is because of multiple scattering points on the surface whose random phase distribution produces interference in a viewing plane. A film record is made of the speckle pattern of a loaded and unloaded test cylinder by a double exposure photographic configuration shown in *Figure 5*. When coherent light is passed through a small region of the film record, a fringe pattern may be observed as shown in *Figure 8*.

The displacement of the region illuminated by the laser beam is inversely proportional to the fringe spacing as given by Equation (5) which is developed later. The direction of displacement for the region is along an axis perpendicular to the fringe orientation. *Figure 9* shows the reconstructed diffraction halo with alternating light and dark bars.

The displacement in the θ direction can be calculated from

$$U = \frac{m\lambda fS}{D} \tag{2}$$

where $U \equiv$ Inplane displacement at a point between loaded and unloaded model

$m \equiv$ Fringe order

$D \equiv$ Spacing between fringes

$\lambda \equiv$ Wavelength of laser illumination source

$f \equiv$ Distance from interferogram to analyzer screen

$S \equiv$ Film scale factor

The vertical, U_V, and the horizontal, U_H components of inplane displacement may be obtained from

$$U_V = \frac{m\lambda fS \sin \Theta}{D} \tag{3}$$

$$U_H = \frac{m\lambda fs \cos \Theta}{D} \tag{4}$$

The complete development of Equation (2) is presented in Mullinix [2]. The wavelength of the HeNe laser light is 6328 Å. The film scale factor, S, is found by dividing the true length of the illuminated cylinder by the image length on the interferogram.

Holographic interferometry was also used to detect surface and subsurface flaws in the composite test cylinders. The test cylinder is placed in one of the illumination beams while the second light beam is a reference beam superimposed on the image from the object at the photographic film plate. Illuminating the processed film plate by a coherent beam resembling the reference beam yields a three dimensional image of the test object. The reconstructed test cylinder contains interference fringe patterns that were created by the change in optical path length due to deformation between the loaded and unloaded states.

B. Data Collection System

The data were collected by an automated laser speckle interferometry displacement contour analyzer developed by John A. Schaeffel, Jr. [3]. The new method of

analyzing laser speckle interferograms uses an off axis optical photodetector developed for generating contour maps of bodies when deformed under load. The photodetector optical geometry is shown in *Figure 10.* Running at 20 percent of maximum speed, the analyzer collects 5000 data points in 4 minutes. *Figure 11* is a photograph of the X-Y translation stage which houses the interferograms. The X-Y stage has the capacity to translate 15 cm in each direction in 0.0025 cm increments with a 0.00025 cm repositioning accuracy. The table is equipped with stepping motors which translate the speckle interferogram in a raster fashion in front of the photodiode which records the light intensity at each point. Contours of minima and maxima intensity were determined and printed in contour fashion on a decwriter. The contour maps represent loci of constant displacement on the body from which the interferogram was made [3]. The direction of displacement is parallel to the axis formed from the central bright spot and the central axis of the photodiode.

Displacement along the direction parallel to the χ axis can be determined from [3]:

$$U_{\chi} = n \left(\frac{S\lambda f}{2\chi}\right) = n\nu \tag{5}$$

where

$$\nu = \left(\frac{S\lambda f}{2\chi}\right) \tag{6}$$

is an optical geometrical constant.

$U\chi$ = Displacement in direction parallel to χ axis.

n = Constant contours where the first minima corresponds to n = 1, the second minima n = 2, etc.

χ = Distance from central bright to center of photodiode

The electrical configuration is shown in *Figure 12. Figure 13* is a photograph of the setup used to obtain the contour mappings. Digital filtering is accomplished by a discrete Fourier transform of the intensity field.

VI. RESULTS

A. Full Field Reconstruction of Speckle Interferograms

A full field interpretation of the fringe patterns was used to determine if the flaws could be detected using speckle interferometry. The full field fringes are obtained by taking optically the Fourier transform of the transmission function [4]. The optical setup for the whole field reconstruction is shown in *Figure 14*. The inplane displacement of the deformed surface is given by:

$$U = (m - \tfrac{1}{2}) \frac{\lambda Z}{Kp} \tag{7}$$

where

U = in plane displacement of cylinder
m = fringe order
λ = wavelength of laser used for illumination
Z = focal length of lens
K = magnification factor
p = distance aperture is offset from focal point of lens

The direction of the displacement is determined by the relation of p with the X and Y axis. The horizontal displacement is measured by moving the aperture along the X axis and the vertical displacement is measured by moving the aperture along the Y axis with the movement starting from the focal point in the transformed plane. Therefore, displacement in any direction can be obtained by the proper selection of the aperture coordinates. In this task the aperture size was selected sufficiently larger so as to completely encompass the flawed region of the cylinder. Photographs of the full field reconstructed speckle interferograms are shown in Appendix A. The cut flawed cylinders did not show any peculiar fringe patterns however the impact flawed cylinders showed very abrupt changes in displacement around the flawed regions. The flawed region was easily detected as can be seen by photograph 83-E-70 (*Figure A 14*) in Appendix A.

B. Full Field Reconstruction of Holograms

Full field reconstruction of holograms was used as a technique to detect surface and subsurface flaws. The optical setup is shown in *Figure 15*. Where the processed film plate is illuminated by a coherent beam at the same angle (α) as the original reference beam, the diffracted rays duplicate the light rays from the test cylinder, and thus an image of the test

object appears in the position it previously occupied. Within the viewing angle subtended by the photographic plate, the hologram provides a full size, three dimensional image of the test cylinder with correct perspective. The image can be examined optically as though it were the original object. Cylinder 7-E-45 *FigureB1* was the only cut flawed cylinder that displayed an irregular fringe pattern as shown in *Figure 16.* However, the impact flaws could be detected in every case. Appendix B shows the photographs of the full field reconstructed holograms of the impact flawed cylinders.

C. Contour Mapping

Contour mapping was performed on selected cylinders with the automated speckle interferometry analyzer system. The cut flawed region in cylinder 7-E-45 was detected using this technique. A contour mapping of the unflawed side of the cylinder is shown in *Figure 17.* While the flawed side of the same cylinder is shown in *Figure 18.* Note the nonuniformity of the contour fringes on the flawed side of the structure. Maxima are indicated by a (-) and minima with a ($). The horizontal row of numbers indicates the scan position across the structure where the vertical column indicates the scan position along the length of the cylinder.

D. Burst Pressure Tests

Each of the composite cylinders was entered into an ultimate pressure testing program. There were nine cut flawed cylinders of each type of material used. One cylinder from each group burst in the flawed location. *Figure 19* is a photograph of a cut flawed cylinder that was pressurized to burst. The E-glass and S-glass cut flawed cylinders had lower average ultimate burst pressures than those cylinders containing no flaws. But there was no significant difference between cut flawed cylinders and nonflawed cylinders made of Kevlar.

Tables 2, 3, and *4* list the cylinders, the type flaws, and burst pressures grouped by the type material. *Figures 20, 21,* and *22* show ultilmate pressure versus wrap single for S-glass and E-glass at 7.2, 9.0, and 10.8 Joules impact energy for 4.8 and 6.4 mm radius dart sizes. In all three cases the greater the amount of energy applied to the cylinder wall the lower the ultimate pressure, as one would expect. In all three cases the ultimate pressure for E-glass was higher at the ±60 degree wrap angle than at the ±45 and ±70 degree wrap angle using the 6.4 mm radius dart. However, this was not the case with 4.8 mm radius dart. Using the 4.8 mm dart on the E-glass cylinder resulted in higher ultimate pressure at the ±70 degree wrap angle than at the ±45 degree and ±60 degree wraps angles. The composite cylinders constructed

from S-glass yielded higher ultimate burst pressures at ±70 degree wrap angle than at ±45 degree and ±60 degree wrap angle and at all three levels of energy regardless of the dart radius size used.

Figures 23, *24*, and *25* show ultimate pressure versus wrap angle for the composite cylinders made of Kevlar at 3.6, 5.4 and 7.2 Joules of impact energy for 4.8 and 6..4 mm dart sizes. In all cases, as the energy level was increased the ultimate burst pressure of the cylinders decreased. At 7.2 Joules of impact energy the ±60 degree wrapped cylinders yielded a higher ultimate pressure than the ±45 degree and ±70 degree wrapped cylinders for both dart sizes. At 3.6 and 5.4 Joules impact energy the ±70 degree wrapped cylinders yielded higher ultimate pressures than the ±45 degree and ±60 degree wrapped cylinders.

Figures 26, *27*, and *28* show ultimate pressure versus impact energy of impact flawed E-glass composite cylinders for ±45 degree, ±60 degree and ±70 degree wrap angle and for 4.8 and 6.4 mm radius darts. *Figures 29, 30,* and *31* show the same information for S-glass and 32, 33, and 34 show the same for Kevlar composite cylinders.

VII. SUMMARY AND CONCLUSIONS

Speckle interferometry and holography were used in flaw detection and evaluation of 108 composite cylinders. Cut fiber and impact flaws were introduced into the walls of E-glass, S-glass, and Kevlar cylinders. Several optical techniques were used to determine surface displacements and detect flaws. The first was an automated laser speckle interferometry displacement contour analyzer. This computer aided system produced contour mappings of the displacement fields obtained from the speckle interferograms. The subcritical flawed regions could be detected using this system. The foremost advantage of this system is the speed at which the data is collected. While operating at 20 percent of capacity, the system collects the data at a rate of 1250 data points per minute. This system not only produces a reconstructed image of the displacement field but also provides the investigator with displacement data.

Full field reconstruction and interpretation of speckle interferograms and holograms was used to detect flaws in the composite structures. The cut flaws could not be detected using full field reconstruction of the speckle interferograms but some could be detected using holography. However the impact flaws were easily detected using full field reconstruction of speckle interferometry and holography as can be seen in the photographs in the appendices.

All of the nondestructive techniques described were found to be effective in detecting critical and subcritical flaws in composite cylinders. The techniques give the investigator a full field displacement picture of the structure as well as displacement data that can be used to determine stresses and strains.

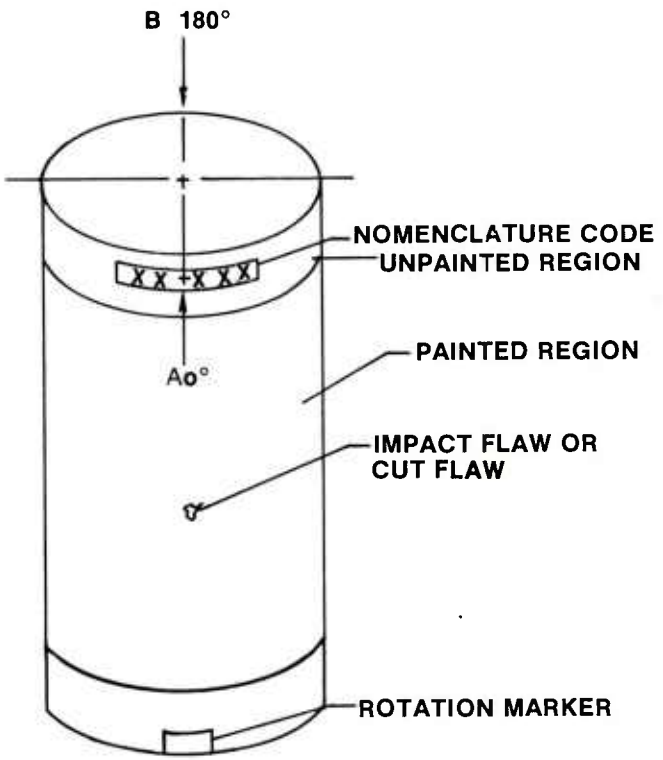

Figure 1. Typical test specimen.

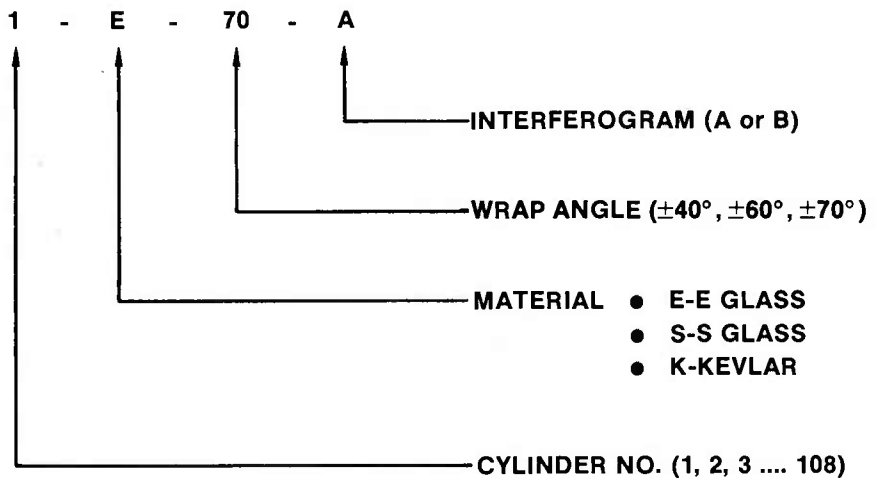

Figure 2. Nomenclature code.

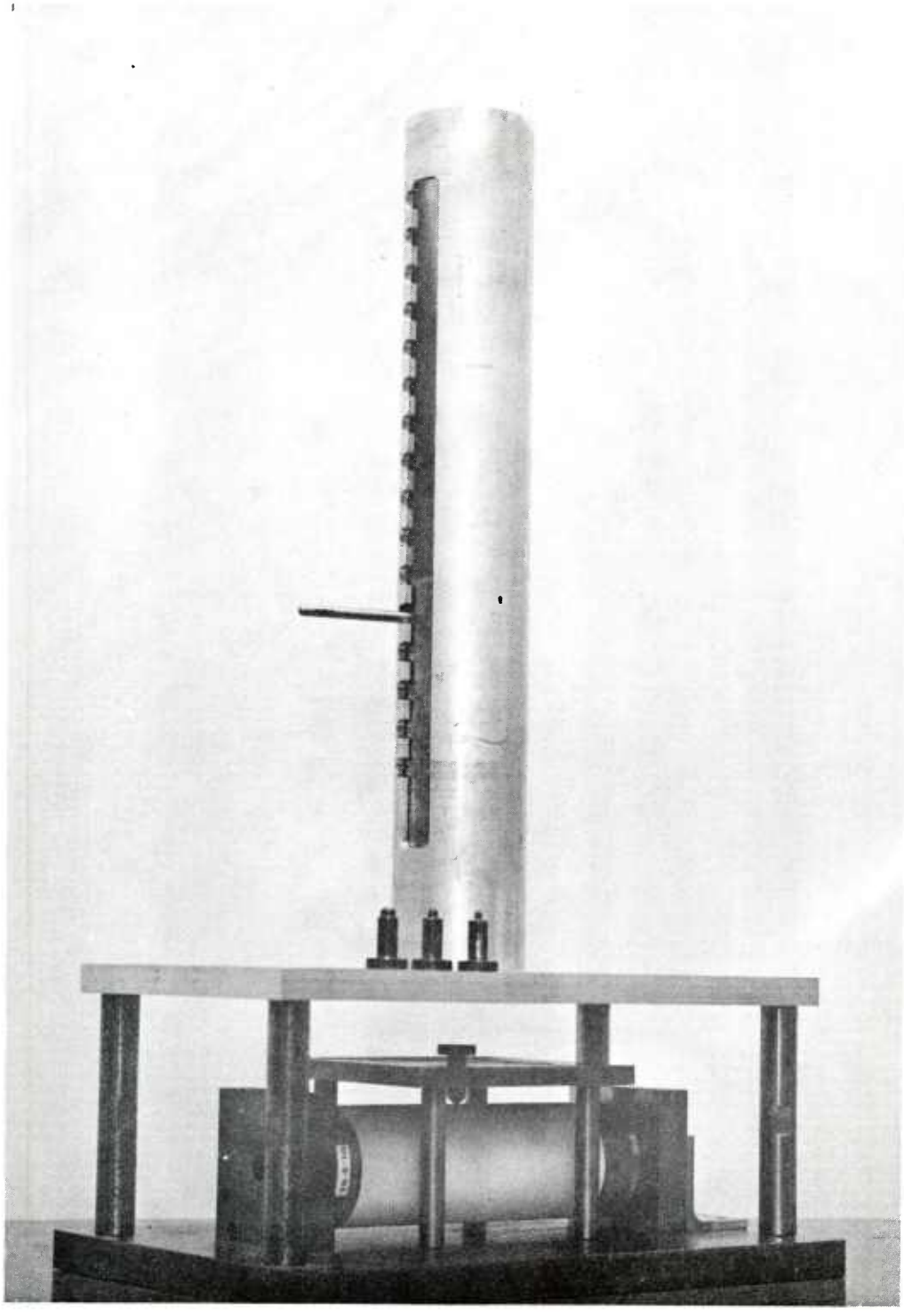

Figure 3. Dynamic impact fixture.

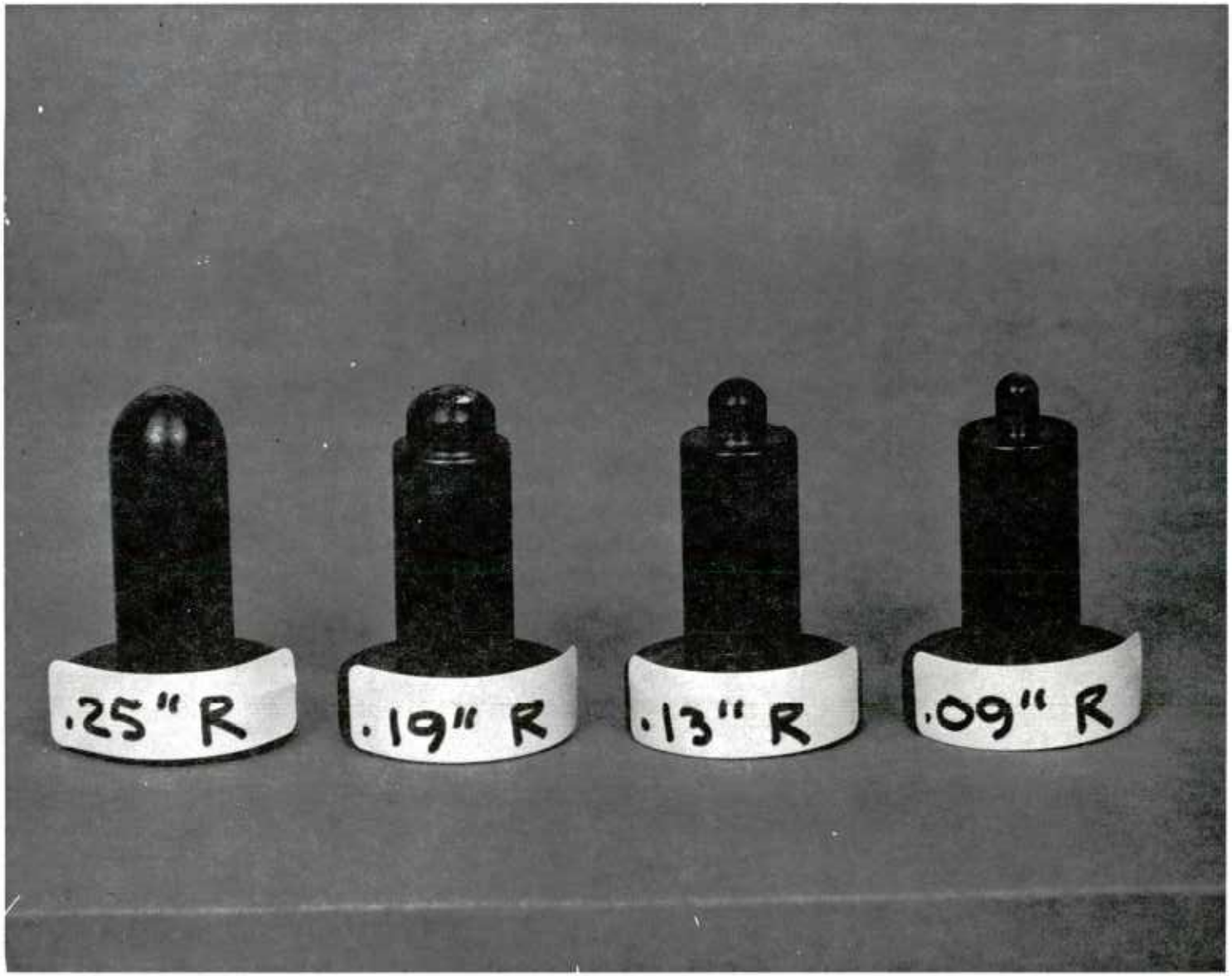

Figure 4. Heat treated darts (dimensions in inches).

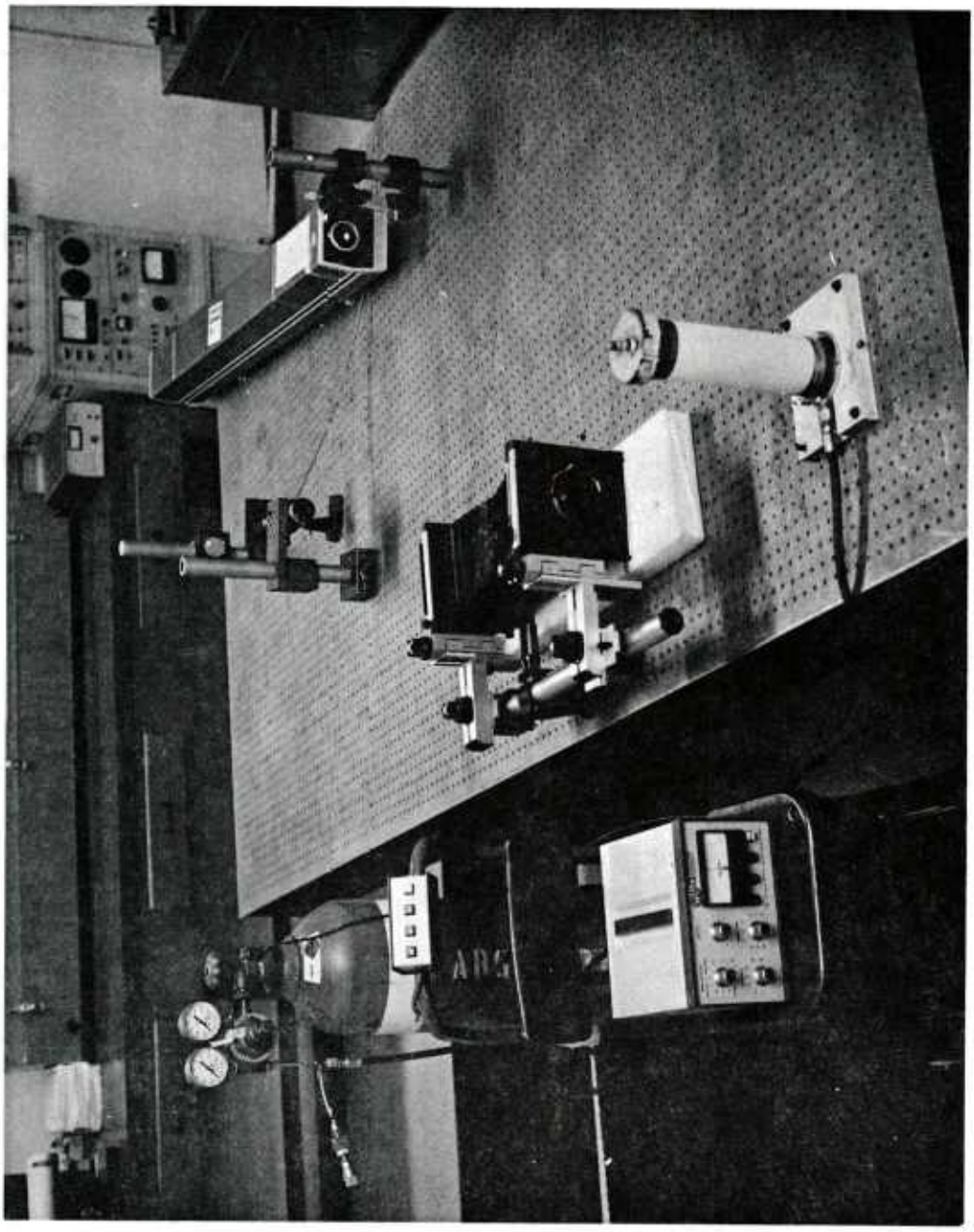

Figure 5. Setup for laser speckle interferometry.

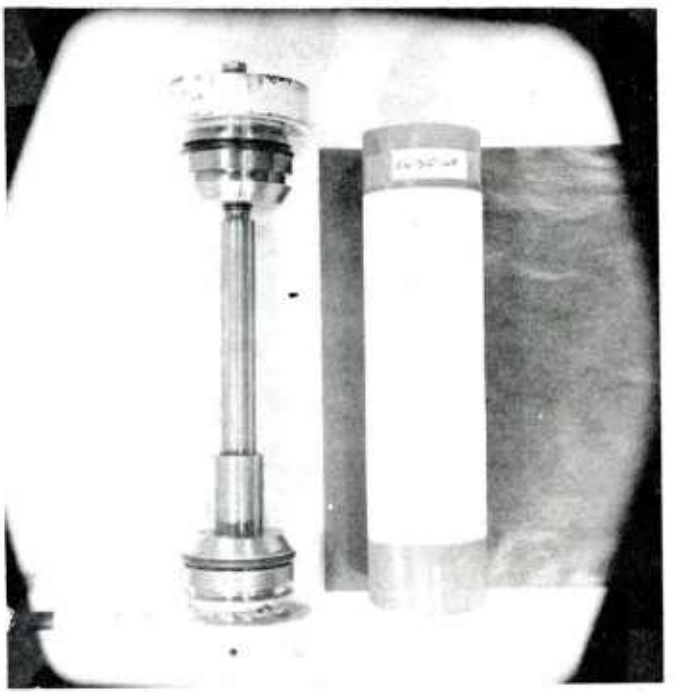

Figure 6. Loading fixture.

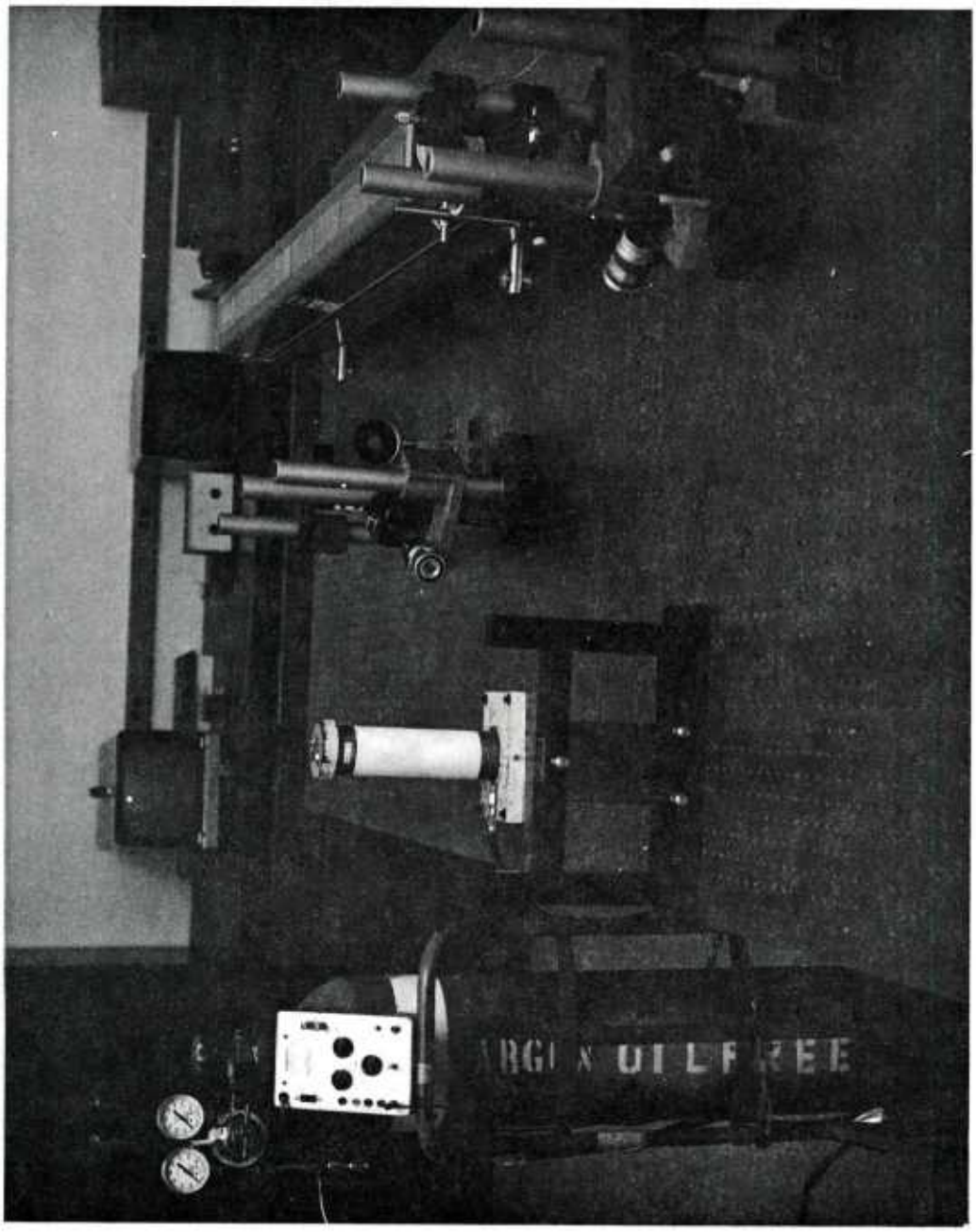

Figure 7. Experimental test setup for holography.

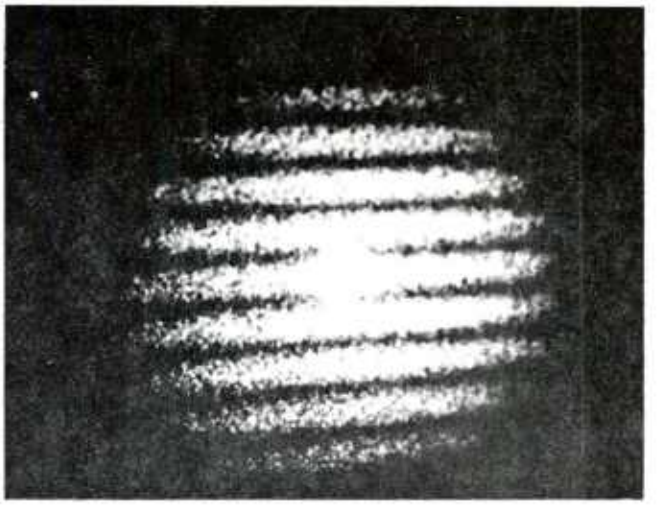

Figure 8. Typical speckel photographic fringe pattern.

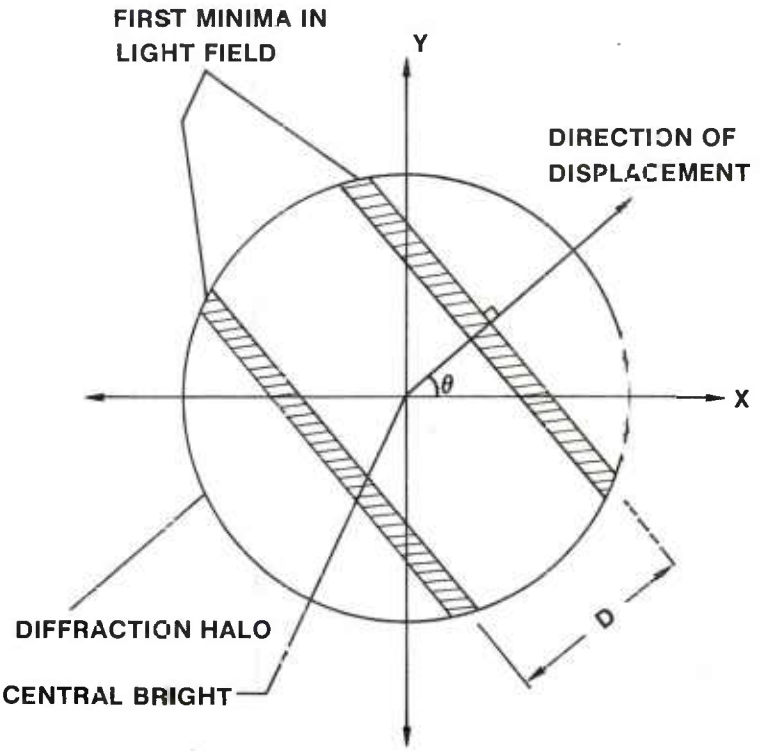

Figure 9. Diffraction halo geometry.

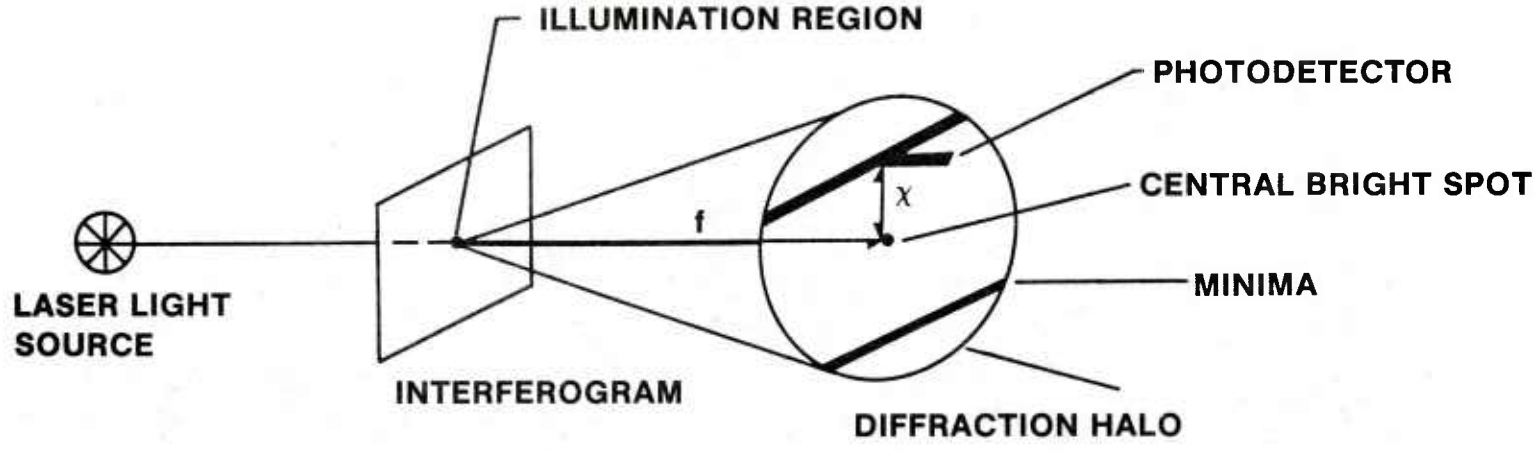

Figure 10. Photodetector optical geometry.

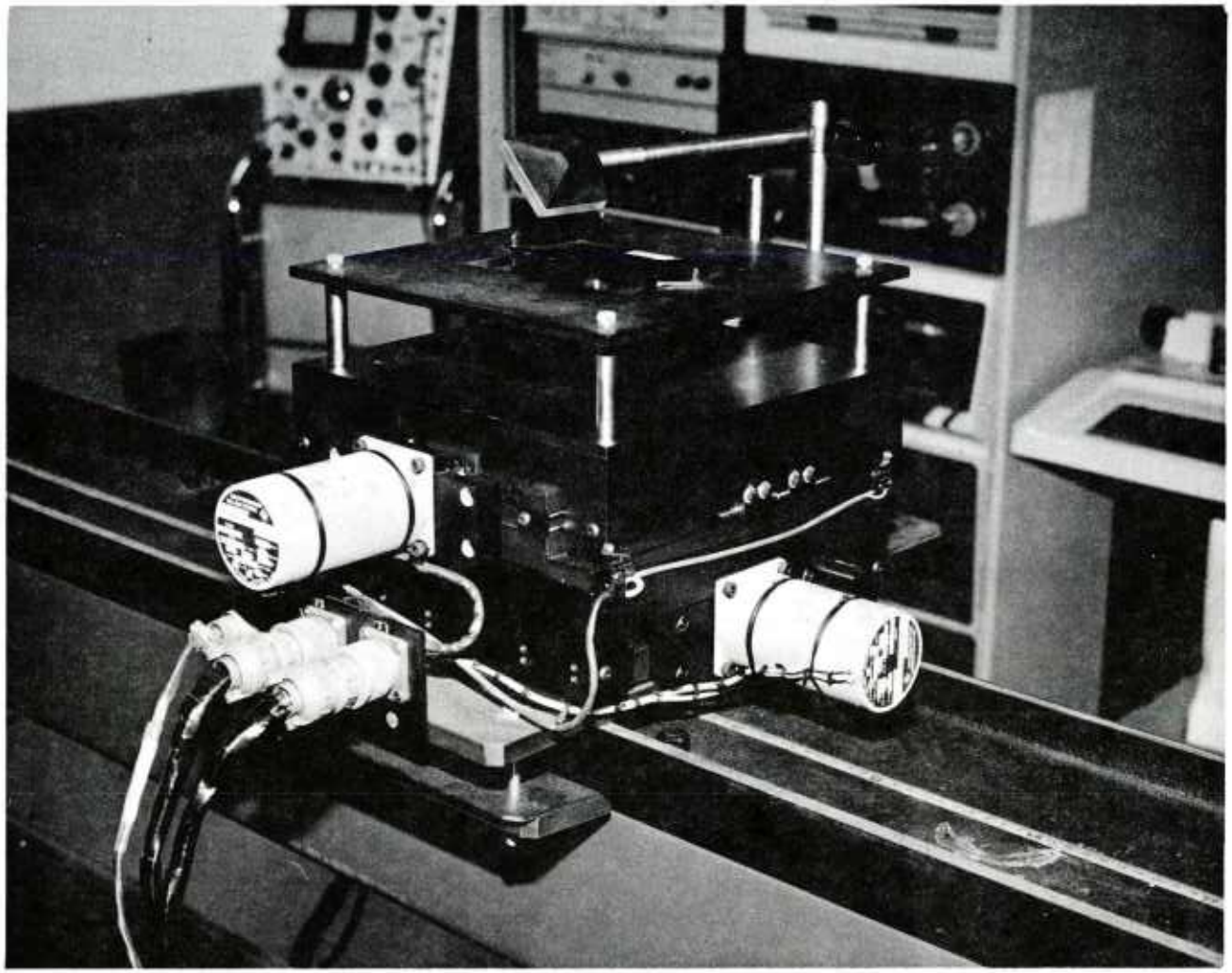

Figure 11. Photograph of the X-Y translation stage.

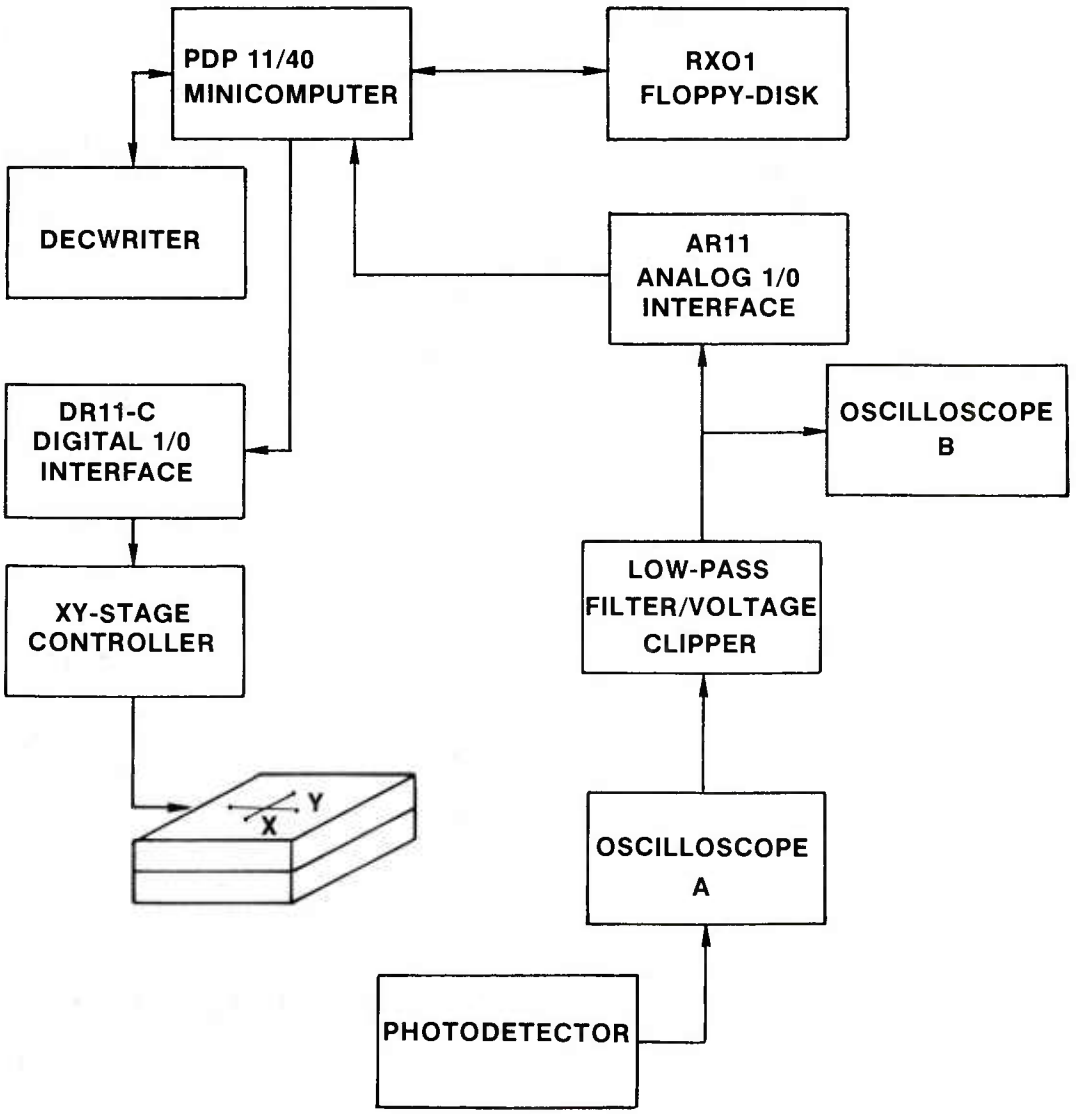

Figure 12. Experimental electrical configuration.

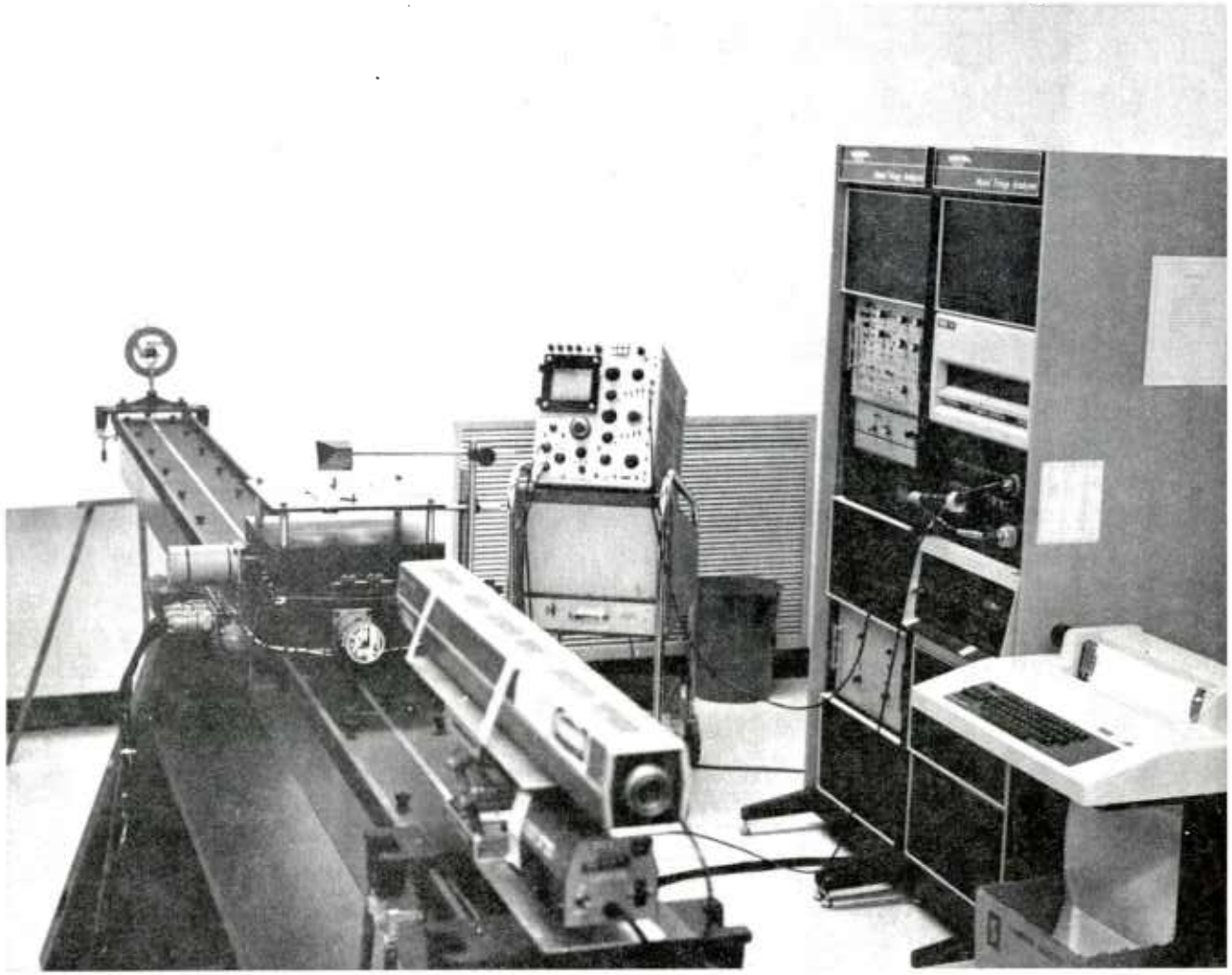

Figure 13. Automated laser speckle interferometry displacement contour analyzer system.

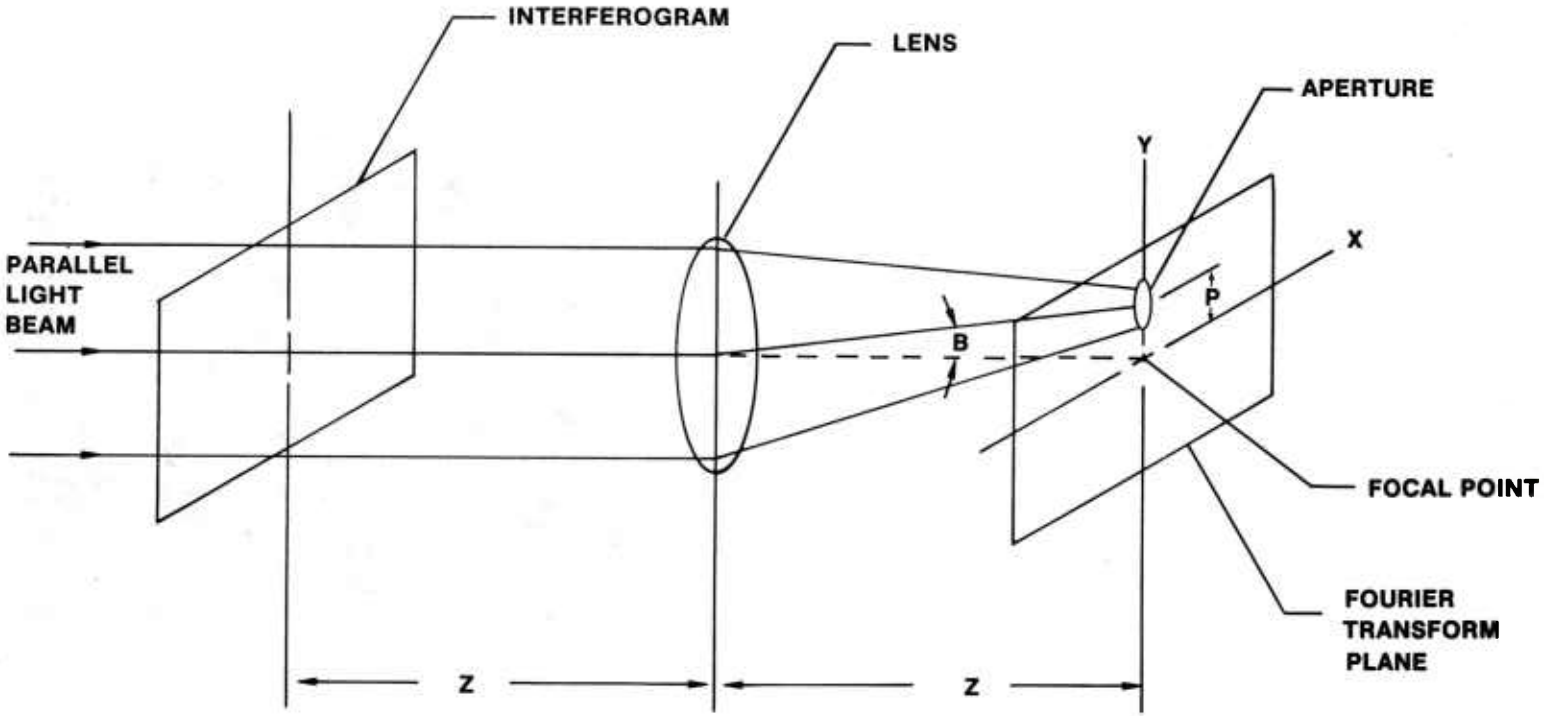

Figure 14. Full field fringe interpretation of interferograms.

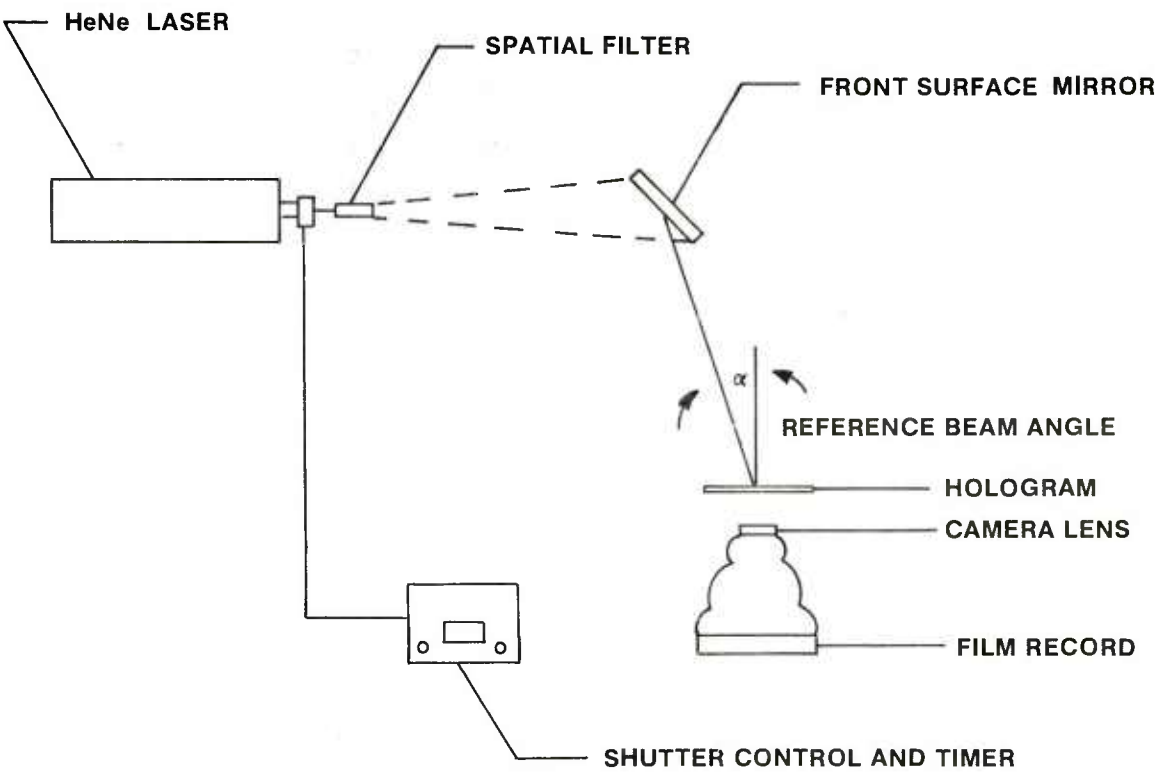

Figure 15. Full field reconstruction of holograms.

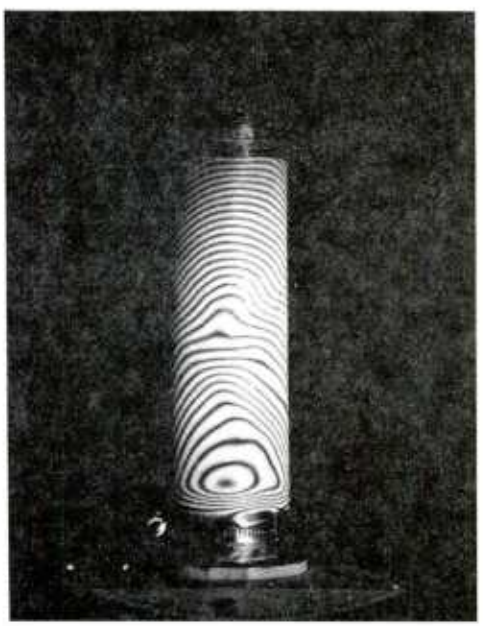

Figure 16. Full field reconstructed hologram of cylinder 7-E-45.

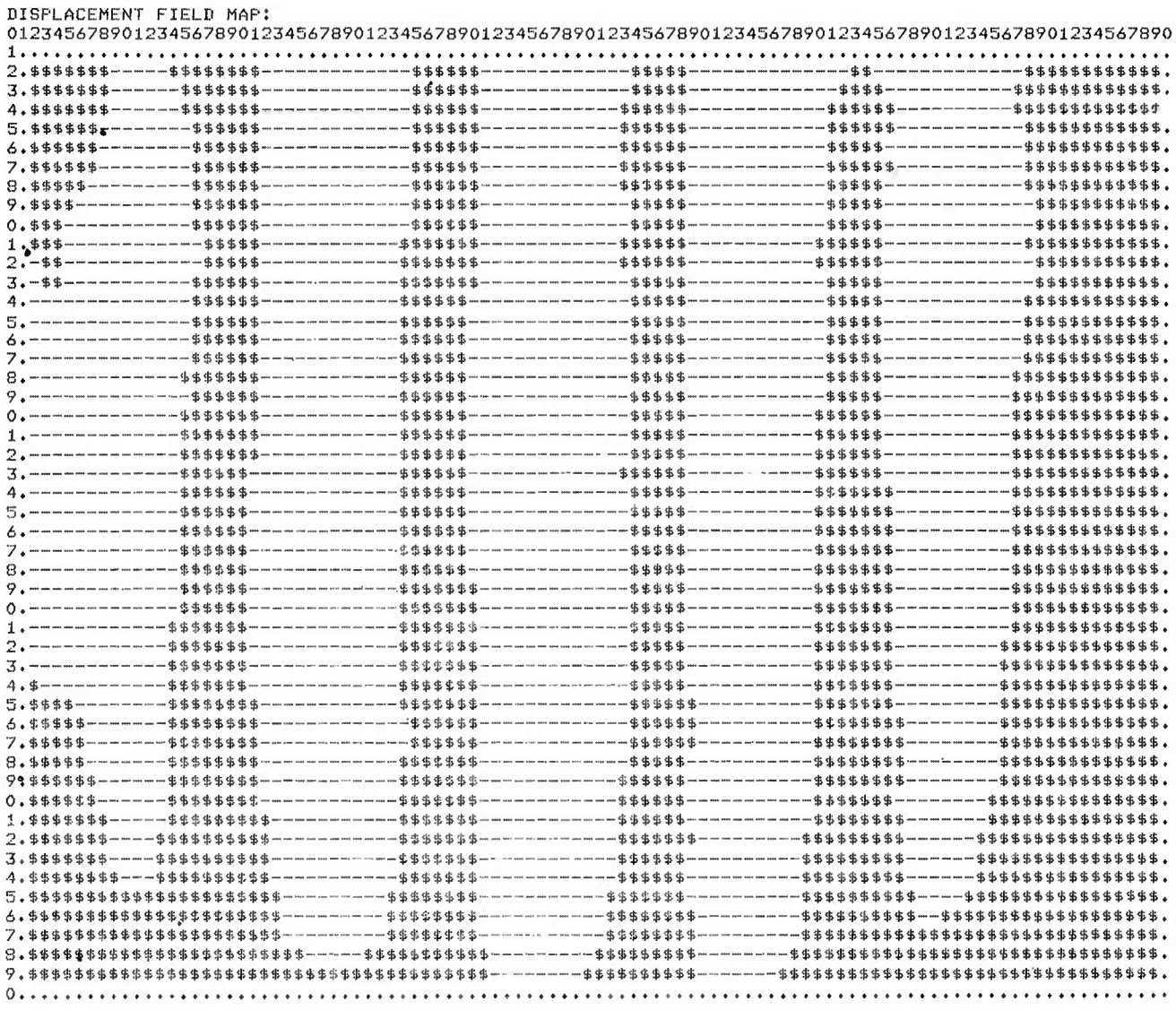

Figure 17. Contour mapping of unflawed side of cylinder 7-E-45.

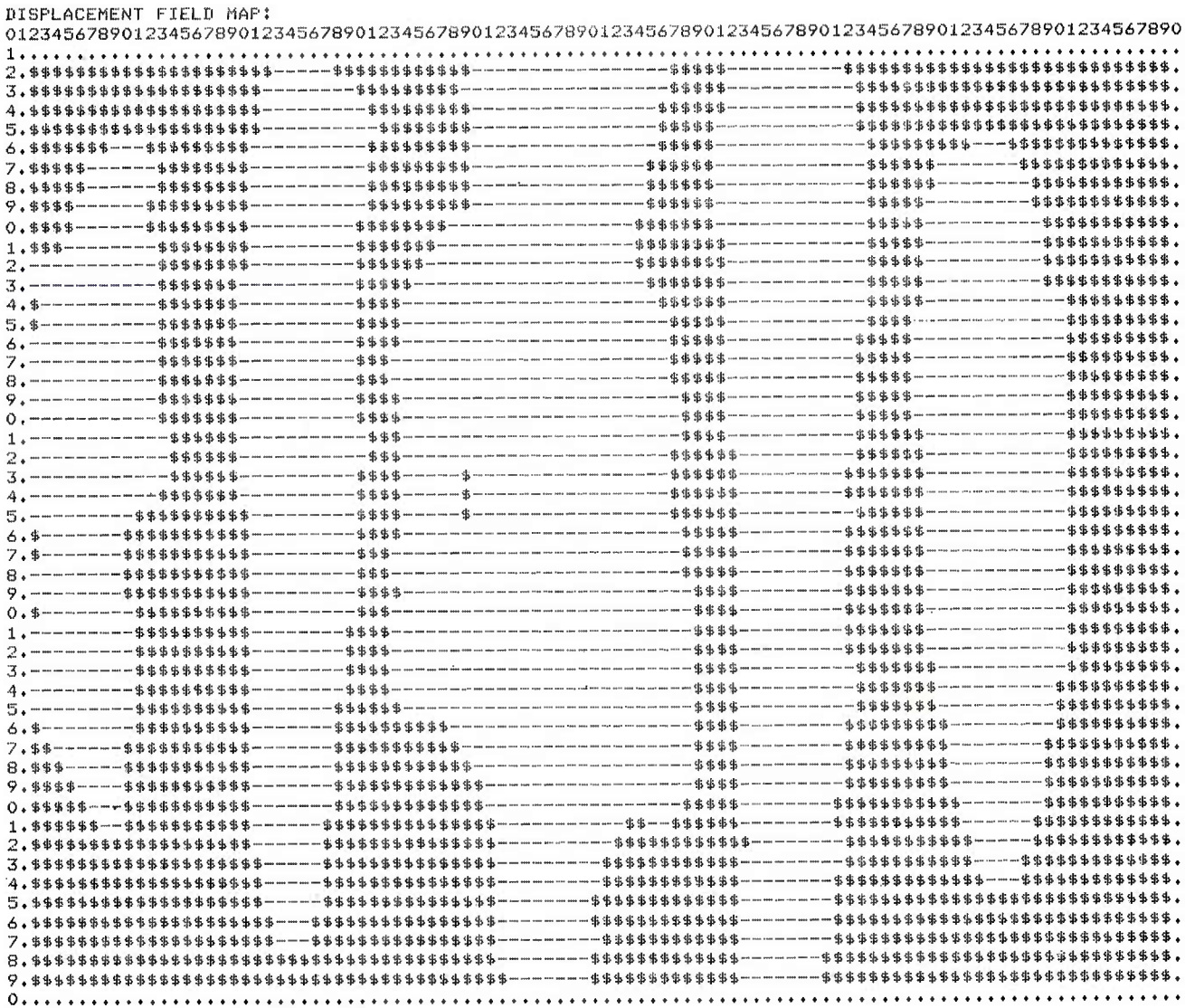

Figure 18. Contour mapping of flawed side of cylinder 7-E-45.

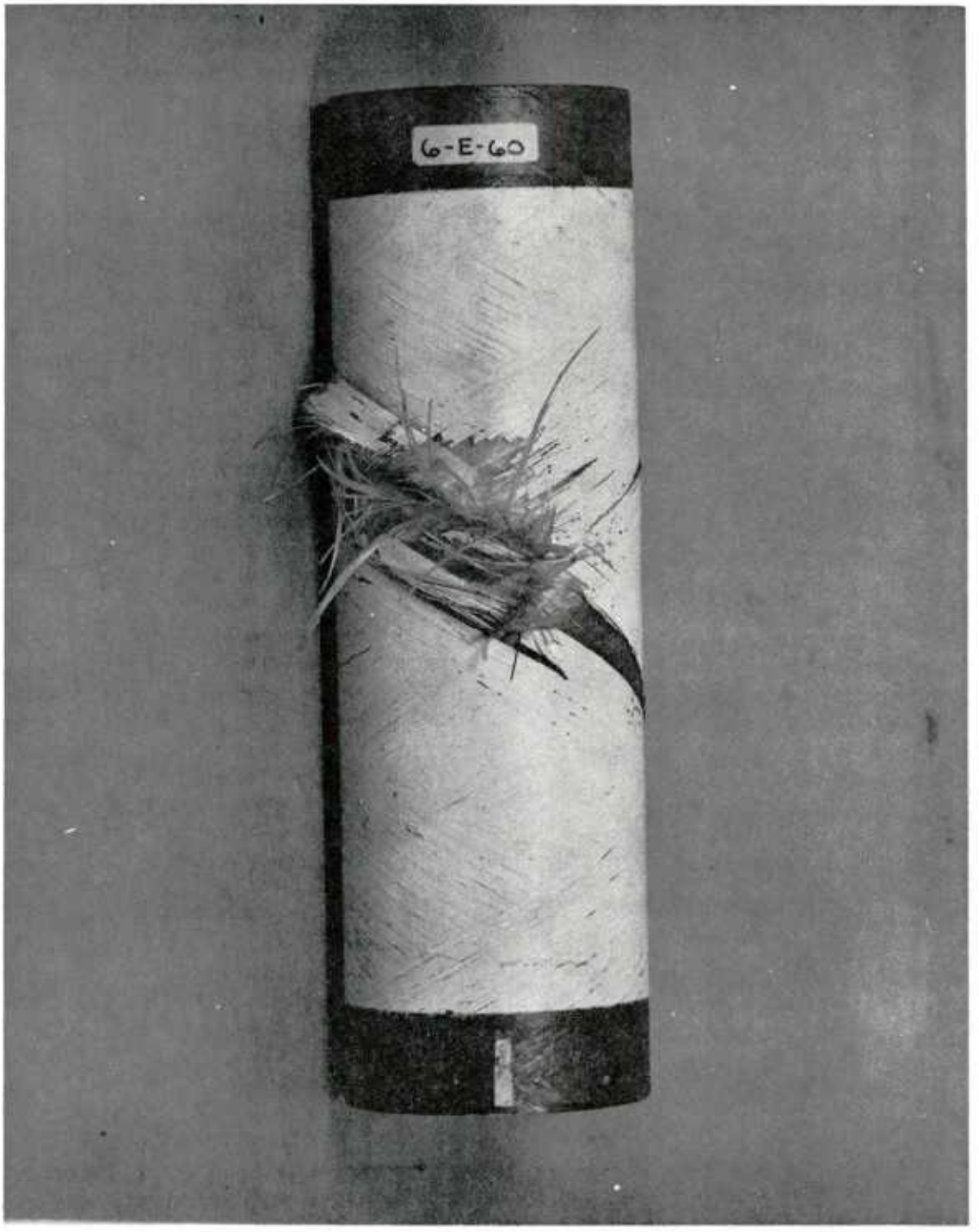

Figure 19. Cut flawed cylinder 6-E-60 pressurized to burst.

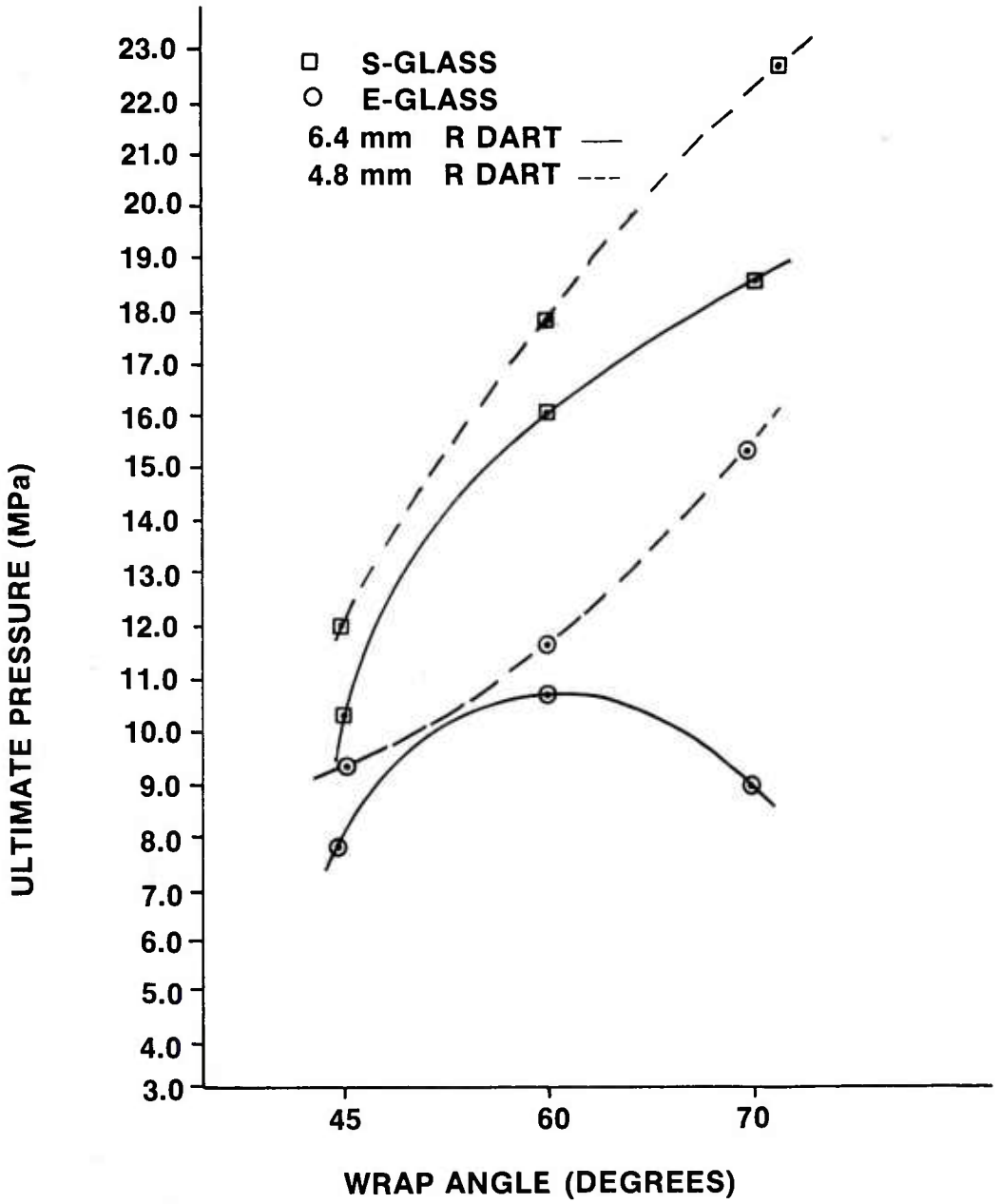

Figure 20. Ultimate pressure versus wrap angle (7.2 Joules (J) impact energy).

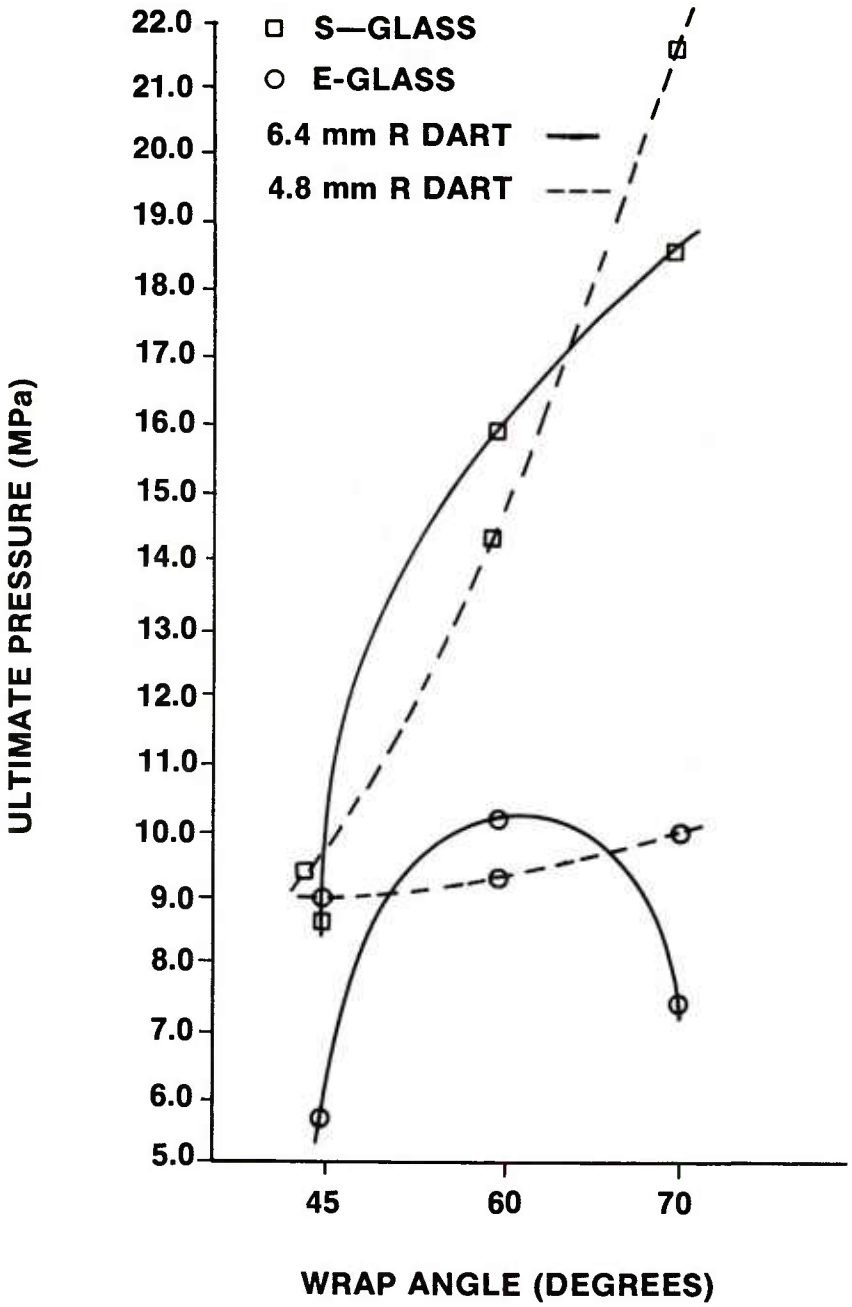

Figure 21. Ultimate pressure versus wrap angle (9.0 J impact energy).

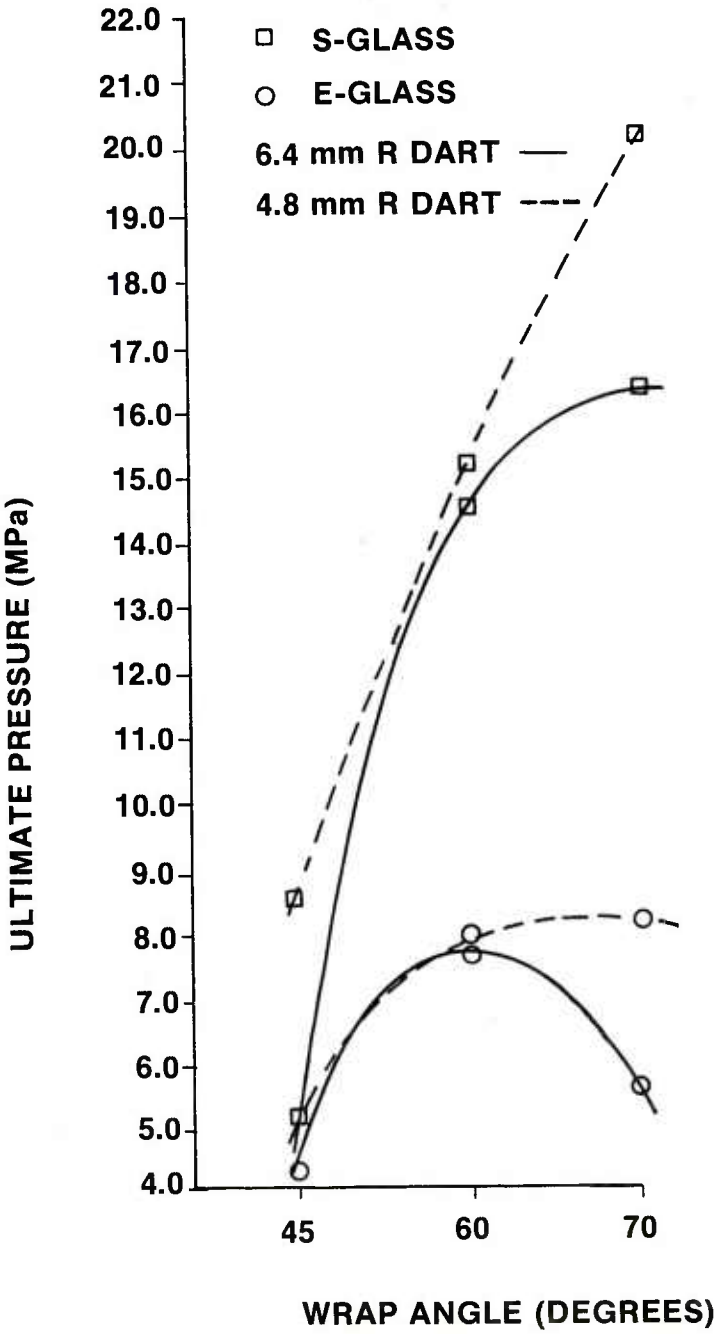

Figure 22. Ultimate pressure versus wrap angle (10.8 J impact energy).

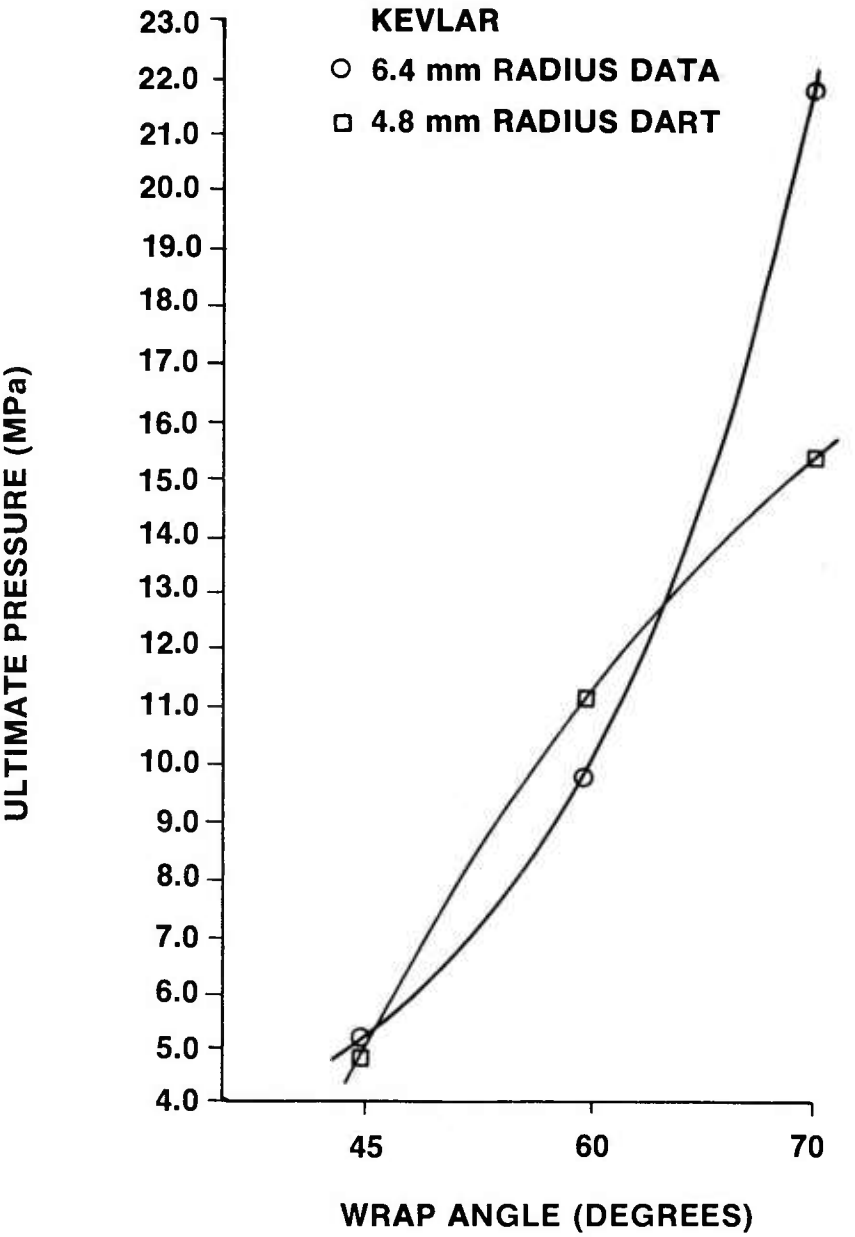

Figure 23. Ultimate pressure versus wrap angle (3.6 J impact energy).

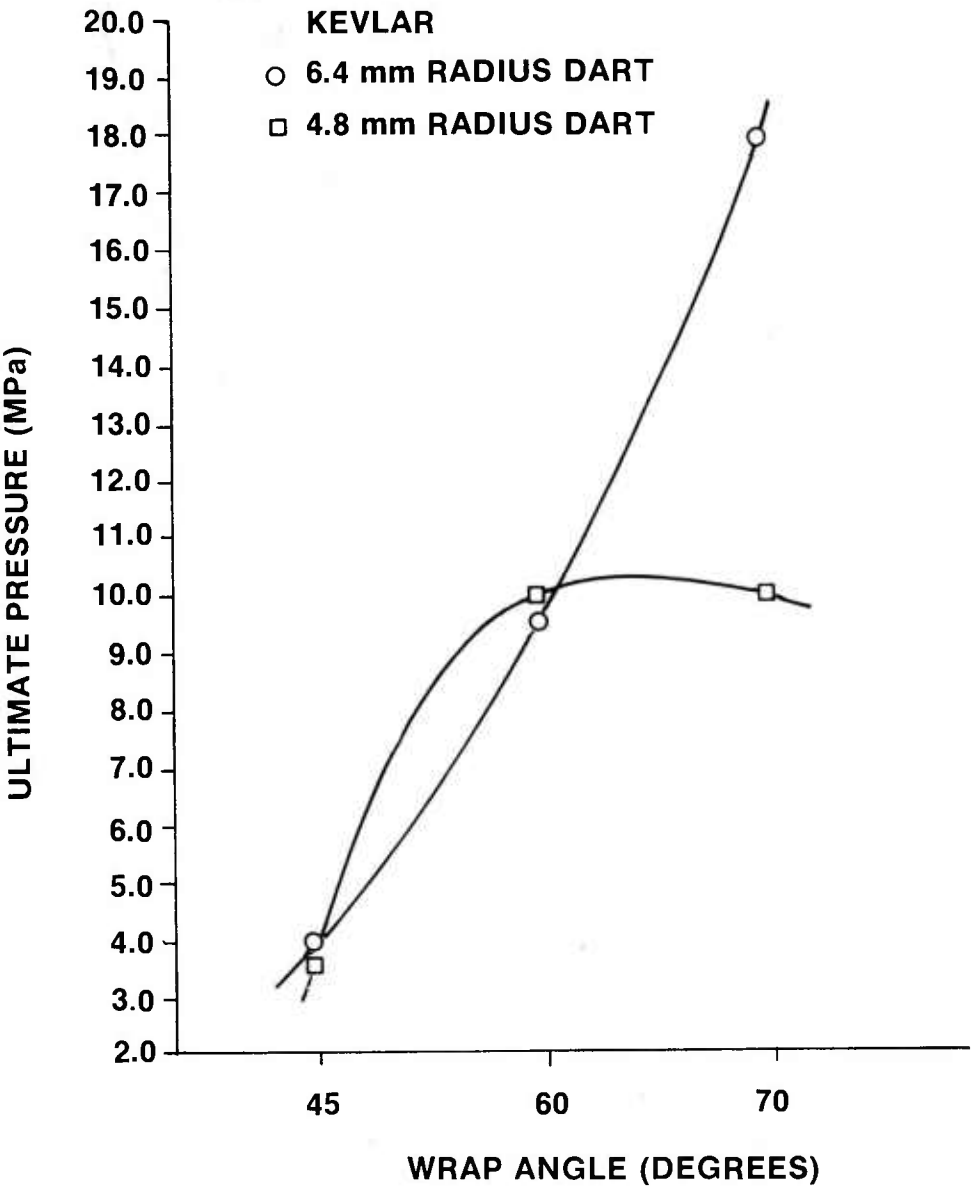

Figure 24. Ultimate pressure versus wrap angle (5.4 J impact energy).

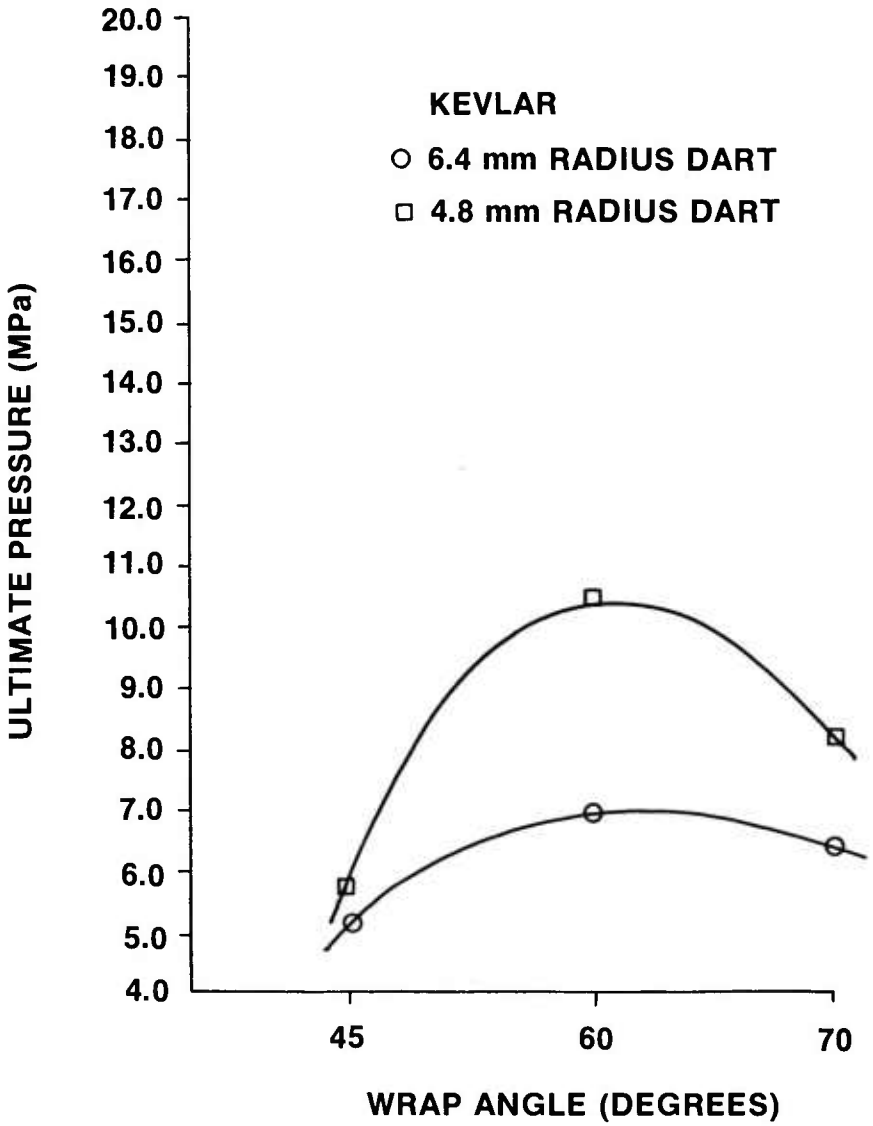

Figure 25. Ultimate pressure versus wrap angle (7.2 J impact energy).

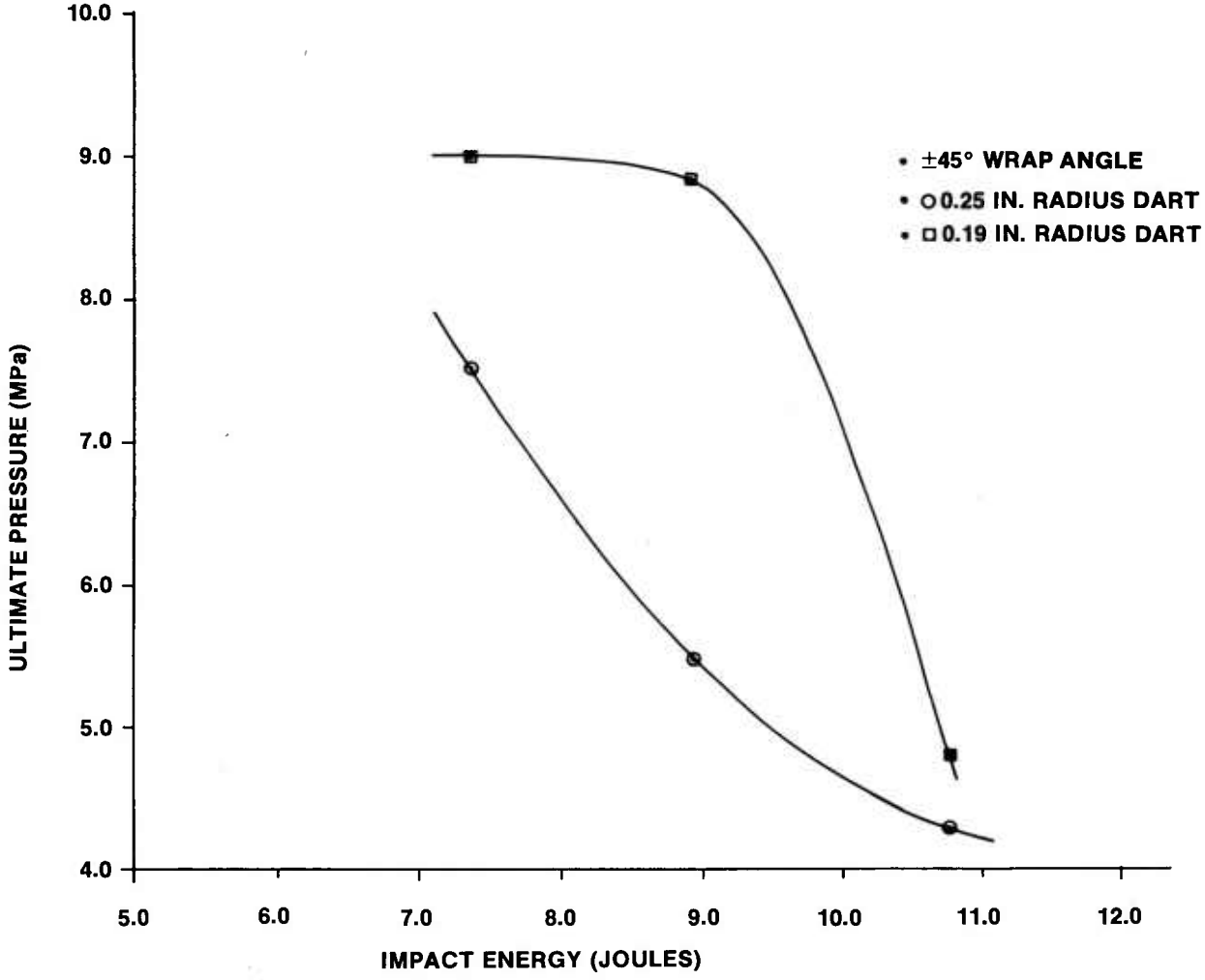

Figure 26. Ultimate pressure versus impact energy (E-glass).

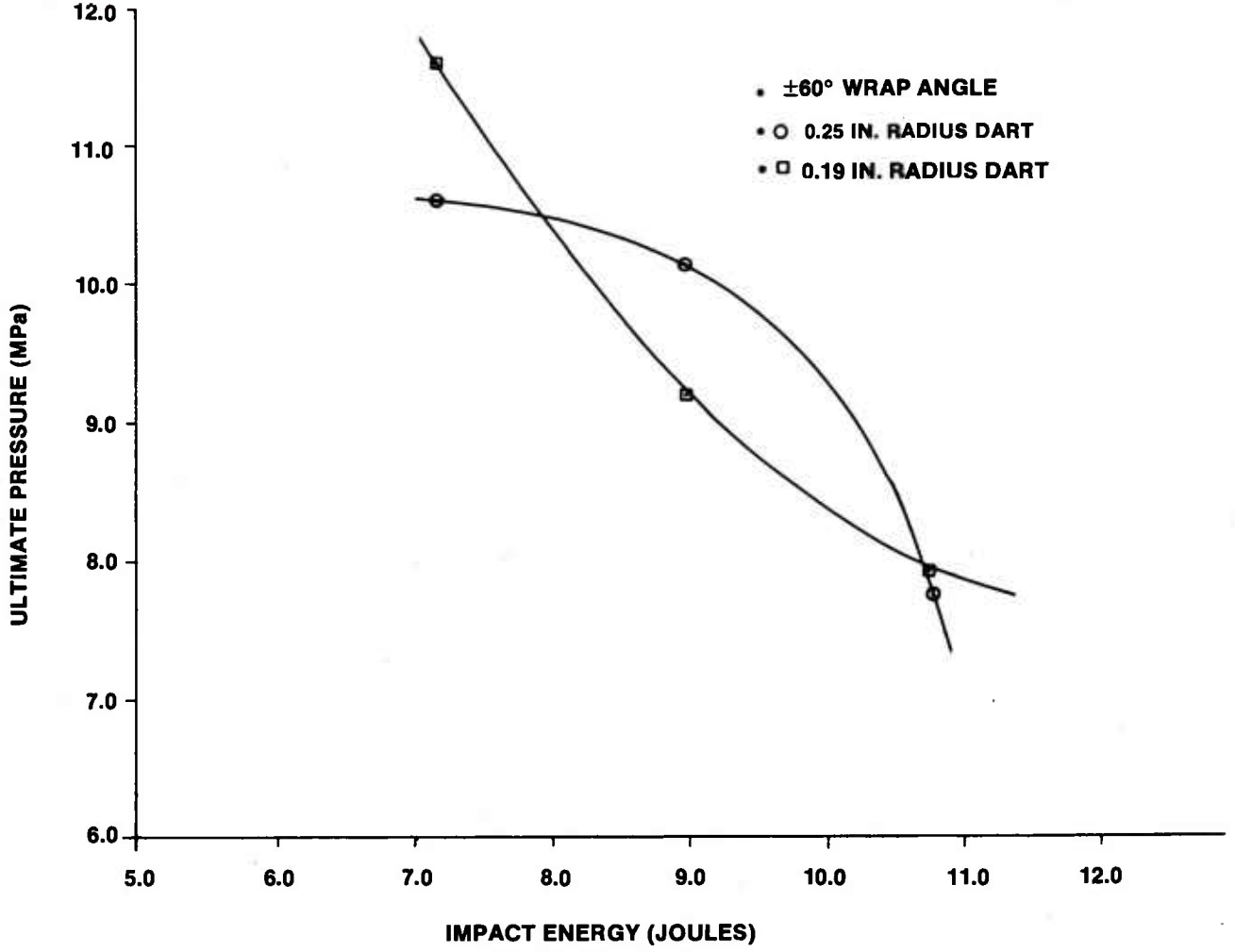

Figure 27. Ultimate pressure versus impact energy (E-Glass).

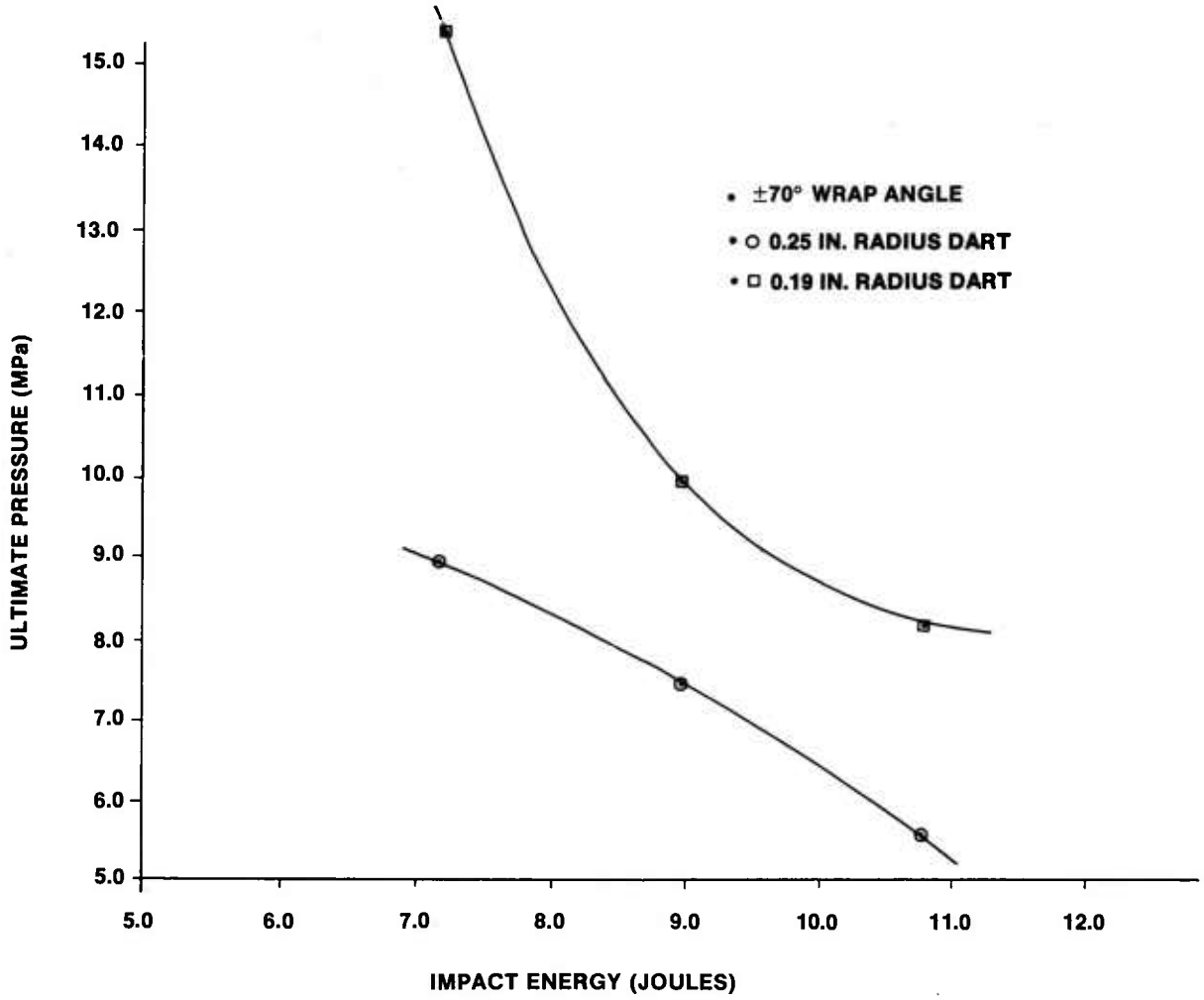

Figure 28. Ultimate pressure versus impact energy (E-glass).

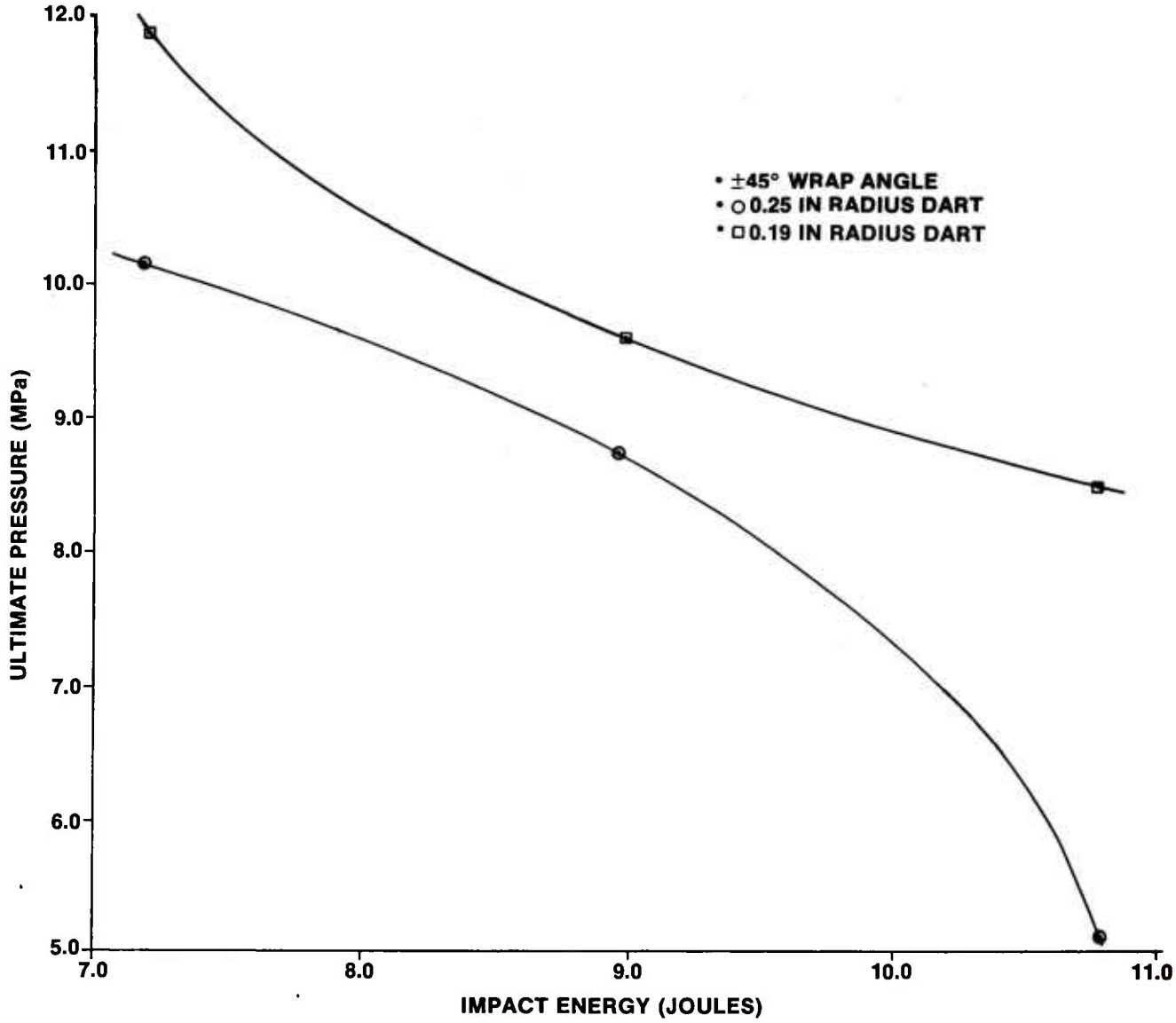

Figure 29. Ultimate pressure versus impact energy (S-glass).

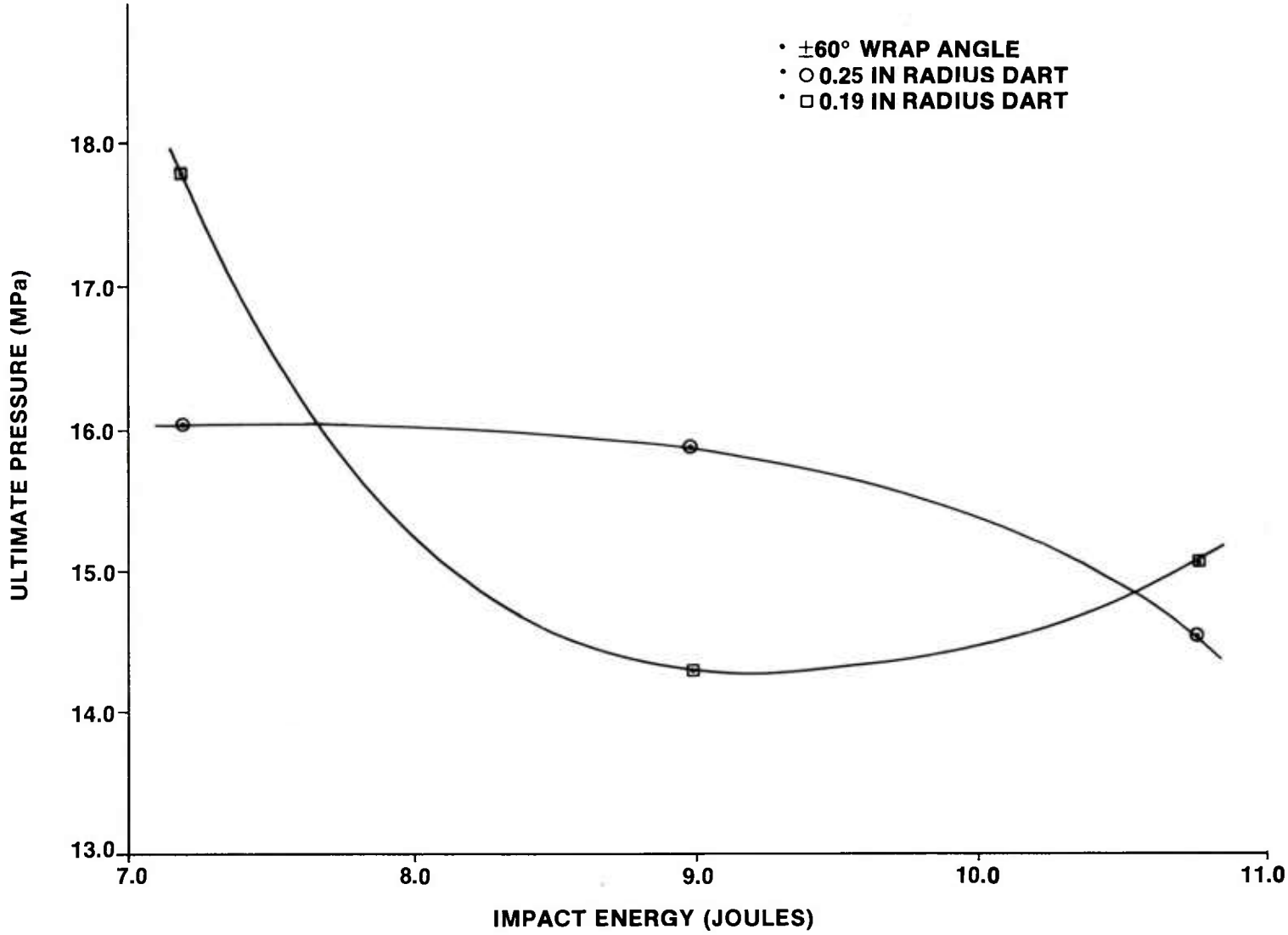

Figure 30. Ultimate pressure versus impact energy (S-glass).

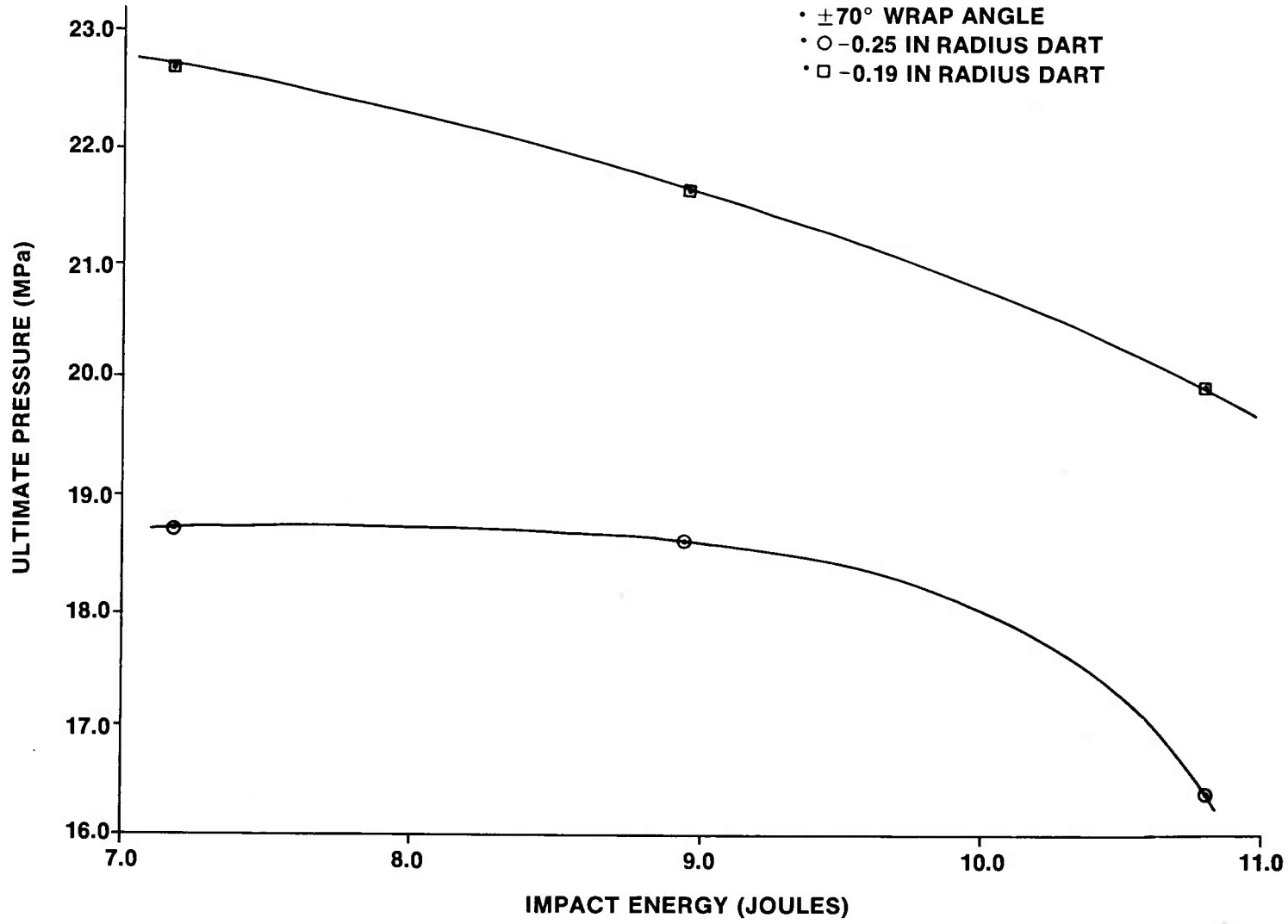

Figure 31. Ultimate pressure versus impact energy (S-glass).

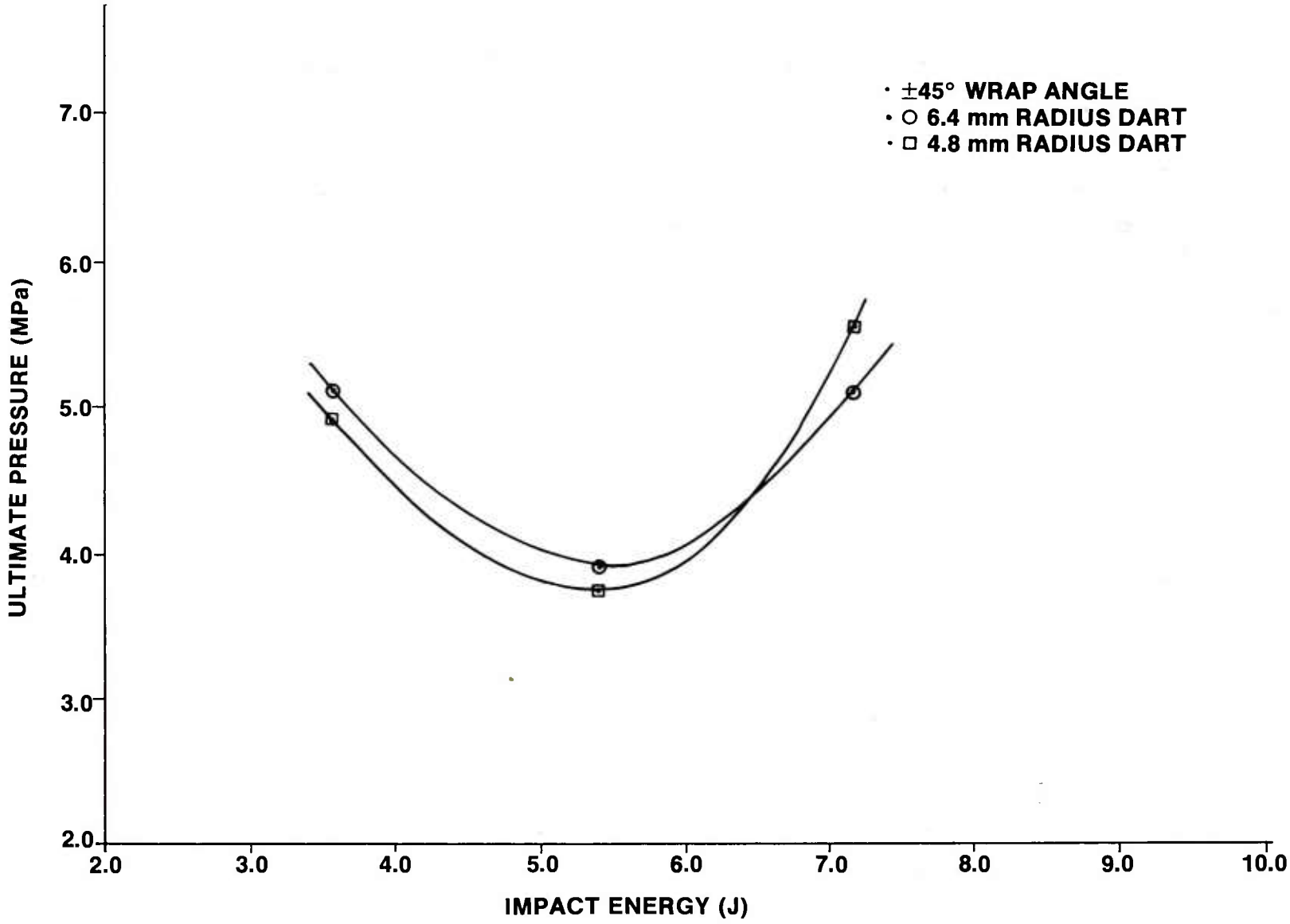

Figure 32. Ultimate pressure versus impact energy (Kevlar).

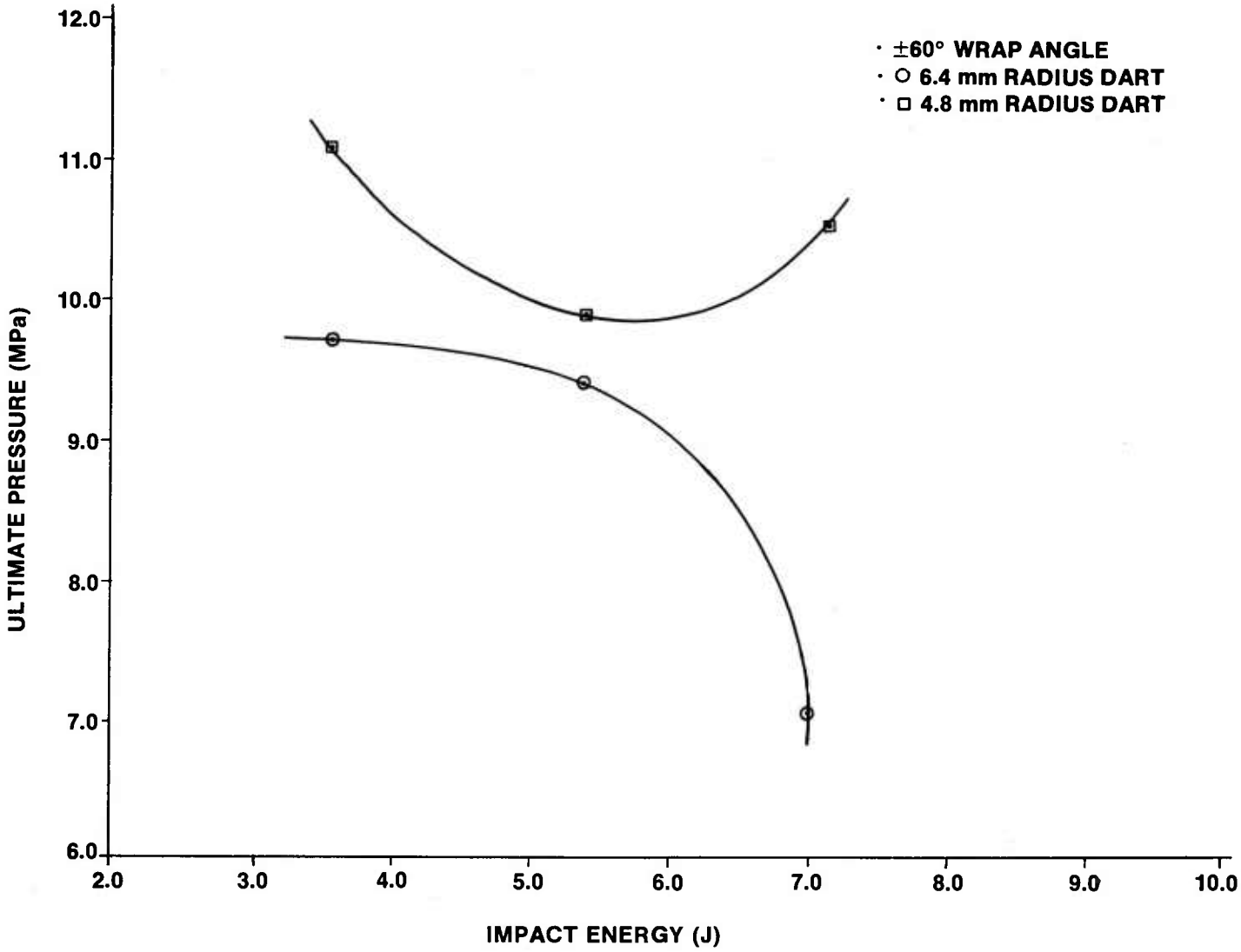

Figure 33. Ultimate pressure versus impact energy (Kevlar).

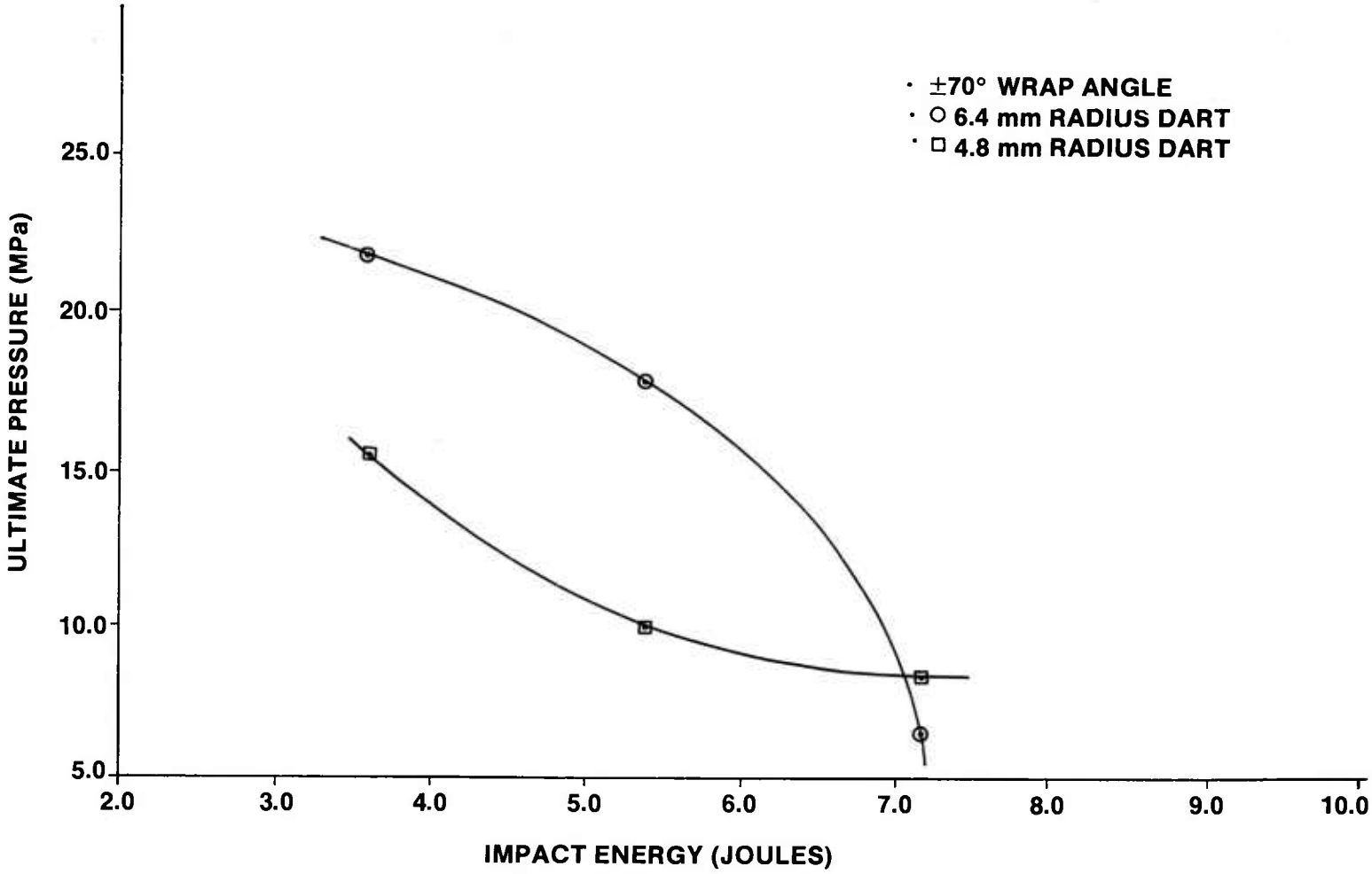

Figure 34. Ultimate pressure versus impact energy (Kevlar).

TABLE 1. TEST CYLINDER LOAD PRESSURE FOR INTERFEROMETRY AND HOLOGRAPHY

MATERIAL	WRAP ANGLE	INTERFEROMETRY LOAD PRESSURE (KPa)	HOLOGRAPHY LOAD PRESSURE (KPa)
E-Glass	±70°	2,240	138
E-Glass	±60°	1,379	103
E-Glass	±45°	1,206	69
S-Glass	±70°	2,240	138
S-Glass	±60°	1,379	103
S-Glass	±45°	1,034	69
Kevlar	±70°	1,206	55
Kevlar	±60°	517	34
Kevlar	±45°	276	28

TABLE 2. LISTING OF E-GLASS BURST PRESSURE AND FLAW TYPE

CYLINDER	TYPE OF FLAW	DART RADIUS SIZE (mm)	AMOUNT OF ENERGY (Joules)	BURST PRESSURE (MPa)
1-E-70	cut			40.6
2-E-70	cut			37.9
3-E-70	cut			39.3
4-E-60	cut			18.3
5-E-60	cut			18.9
6-E-60	cut			18.9
7-E-45	cut			6.4
8-E-45	cut			8.4
9-E-45	cut			9.9
19-E-70	impact	6.4	7.19	8.9
20-E-70	impact	6.4	9.00	7.3
21-E-70	impact	6.4	10.80	5.7
22-E-60	impact	6.4	7.19	6.8
23-E-60	impact	6.4	10.80	7.4
24-E-60	impact	6.4	5.40	7.2
25-E-45	impact	6.4	7.19	7.5
26-E-45	impact	6.4	9.00	4.3
27-E-45	impact	6.4	10.80	5.4
37-E-70	none			41.0
38-E-70	none			39.7
39-E-70	none			39.5
40-E-60	impact	6.4	7.19	10.6
41-E-60	impact	6.4	9.00	10.2
42-E-60	impact	6.4	10.80	7.7
43-E-45	none			9.5
44-E-45	none			6.1
45-E-45	none			9.2
82-E-70	impact	4.8	7.19	15.4
83-E-70	impact	4.8	9.00	9.9
84-E-70	impact	4.8	10.80	8.1
85-E-60	impact	4.8	7.19	11.6
86-E-60	impact	4.0	9.00	9.2
87-E-60	impact	4.8	10.80	7.9
88-E-45	impact	4.8	7.19	9.0
89-E-45	impact	4.8	9.00	8.9
90-E-45	impact	4.8	10.80	4.8

TABLE 3. LISTING OF S-GLASS BURST PRESSURE AND FLAW TYPE

CYLINDER	TYPE OF FLAW	DART RADIUS SIZE (mm)	AMOUNT OF ENERGY (Joules)	BURST PRESSURE (MPa)
10-S-70	cut			48.1
11-S-70	cut			43.4
12-S-70	cut			43.7
13-S-60	cut			26.6
14-S-60	cut			23.0
15-S-60	cut			24.9
16-S-45	cut			12.6
17-S-45	cut			10.3
18-S-45	cut			12.3
28-S-70	impact	6.4	7.19	18.6
29-S-70	impact	6.4	9.00	18.6
30-S-70	impact	6.4	10.80	16.4
31-S-60	impact	6.4	3.59	20.1
32-S-60	impact	4.8	3.59	17.7
33-S-60	impact	4.8	3.59	17.4
34-S-45	impact	6.4	7.19	10.2
35-S-45	impact	6.4	9.00	8.7
36-S-45	impact	6.4	10.80	5.1
46-S-70	none			47.0
47-S-70	none			48.6
48-S-70	none			48.9
49-S-60	impact	6.4	7.19	16.0
50-S-60	impact	6.4	9.00	15.9
51-S-60	impact	6.4	9.00	14.6
52-S-45	none			12.2
53-S-45	none			9.7
54-S-45	none			14.1
91-S-70	impact	4.8	7.19	22.7
92-S-70	impact	4.8	9.00	21.6
93-S-70	impact	4.8	10.80	20.2
94-S-60	impact	4.8	7.19	17.8
95-S-60	impact	4.8	9.00	14.3
96-S-60	impact	4.8	10.80	15.1
97-S-45	impact	4.8	7.19	11.9
98-S-45	impact	4.8	9.00	9.6
99-S-45	impact	4.8	10.80	8.5

TABLE 4. LISTING OF KEVLAR BURST PRESSURE AND FLAW TYPE

CYLINDER	TYPE OF FLAW	DART RADIUS SIZE (mm)	AMOUNT OF ENERGY (Joules)	BURST PRESSURE (MPa)
55-K-70	cut			30.7
56-K-70	cut			27.8
57-K-70	cut			23.5
58-K-60	cut			9.9
59-K-60	cut			9.4
60-K-60	cut			10.2
61-K-45	cut			6.5
62-K-45	cut			4.8
63-K-45	cut			7.0
64-K-70	impact	6.4	3.59	21.8
65-K-70	impact	6.4	5.40	17.9
66-K-70	impact	6.4	7.19	6.4
67-K-60	impact	6.4	3.59	9.7
68-K-60	impact	6.4	5.40	9.4
69-K-60	impact	6.4	7.19	7.0
70-K-45	impact	6.4	3.59	5.1
71-K-45	impact	6.4	5.40	3.9
72-K-45	impact	6.4	7.19	5.1
73-K-70	impact	4.8	1.80	24.4
74-K-70	none			24.3
75-K-70	none			24.9
76-K-60	impact	4.8	3.59	11.1
77-K-60	impact	4.8	5.40	9.9
78-K-60	impact	4.8	7.19	10.5
79-K-45	impact	4.8	3.59	4.9
80-K-45	impact	4.8	5.40	3.7
81-K-45	impact	4.8	7.19	5.6
100-K-70	impact	4.8	7.19	20.7
101-K-70	impact	4.8	9.00	15.8
102-K-70	impact	4.8	10.80	15.4
103-K-60	none			11.2
104-K-60	none			11.2
105-K-60	none			11.8
106-K-45	none			5.8
107-K-45	none			4.4
108-K-45	none			6.4

REFERENCES

1. Vandiver, T. L., Determination of Elastic Constants for Flawed and Unflawed Composite Tubes Using Speckle Interferometry, US Army Missile Command, Redstone Arsenal, Alabama, Technical Report T-79-36, 8 March 1979.

2. Mullinix, B. R., Ranson, W. F., Swinson, W. F., and Cost, T. L., Quantification of Flaws in Fibered Composite Structures Using Interferometric Fringe Patterns, US Army Missile Command, Redstone Arsenal, Alabama, Technical Report RL-76-18, 20 April 1976.

3. Schaeffel, J. A., Automated Laser Speckle Interferometry Displacement Contour Analyzer, US Army Missile Command, Redstone Arsenal, Alabama, Technical Report T-79-71, 2 July 1979.

4. Wilson, T. F., "Determination of In-Plane Displacement Using Speckle Interferometry", Master of Science Thesis, Department of Mechanical Engineering, Auburn University, 7 June 1977.

APPENDIX A

FULL FIELD RECONSTRUCTED INTERFEROGRAMS

Figure A 1. Test cylinder 20-E-70.

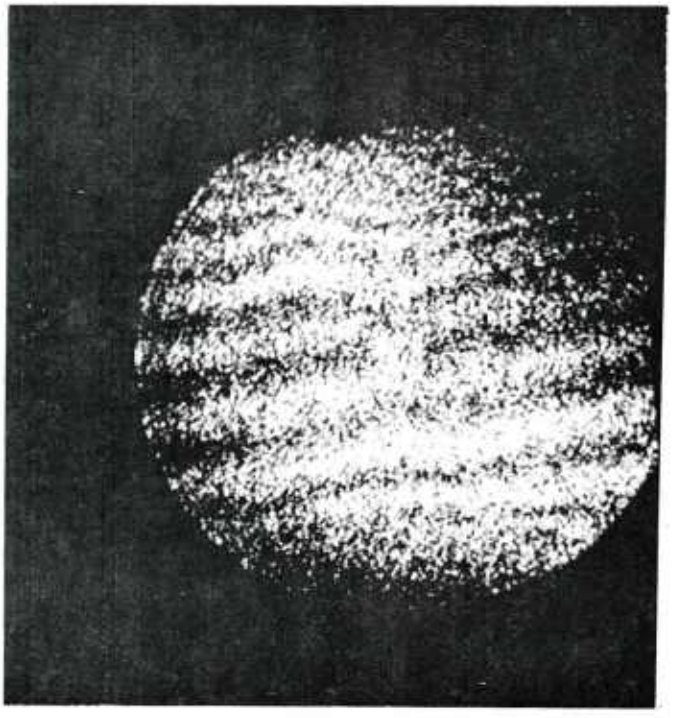

Figure A 2. Test cylinder 30-S-70

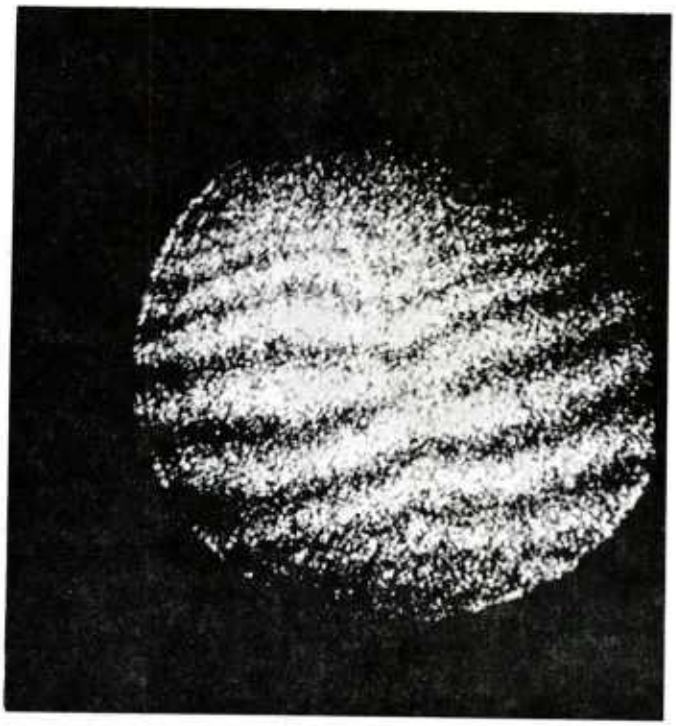

Figure A 3. Test cylinder 40-E-60.

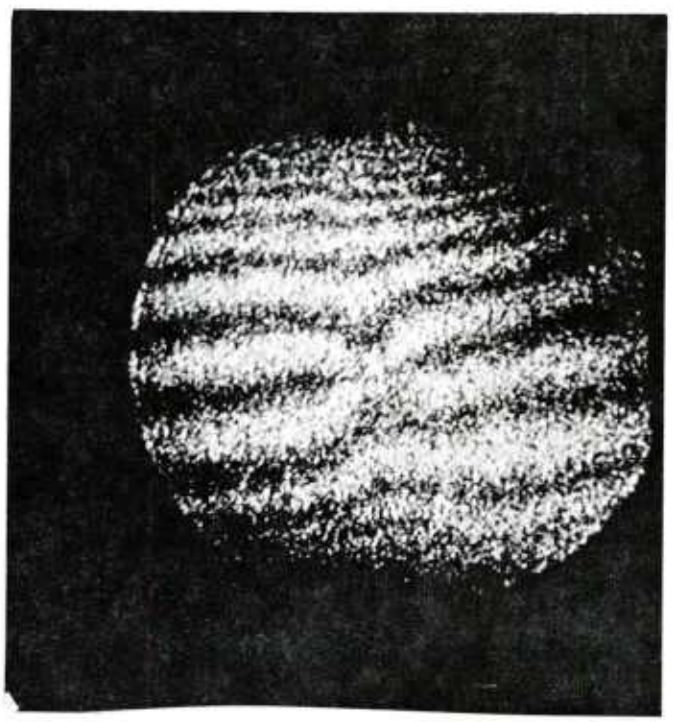

Figure A 4. Test cylinder 41-E-60.

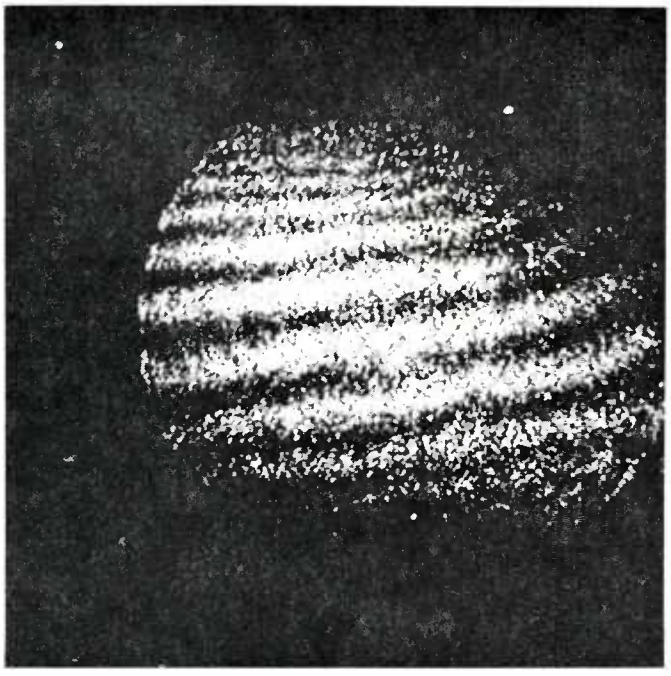

Figure A 5. Test cylinder 42-E-60.

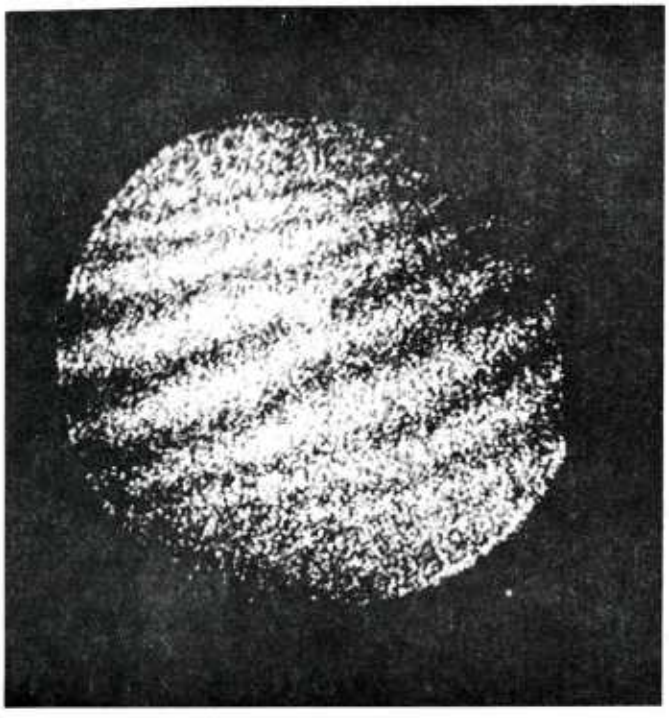

Figure A 6. Test cylinder 51-S-60.

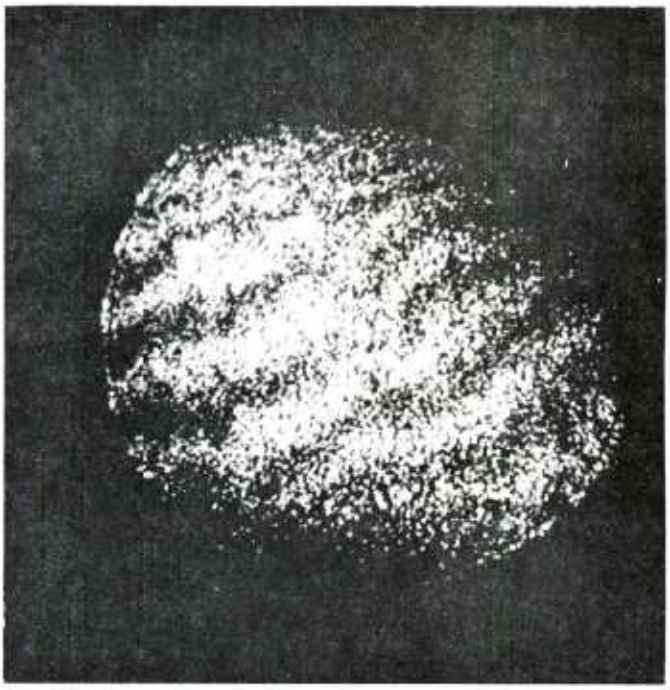

Figure A 7. Test cylinder 64-K-70.

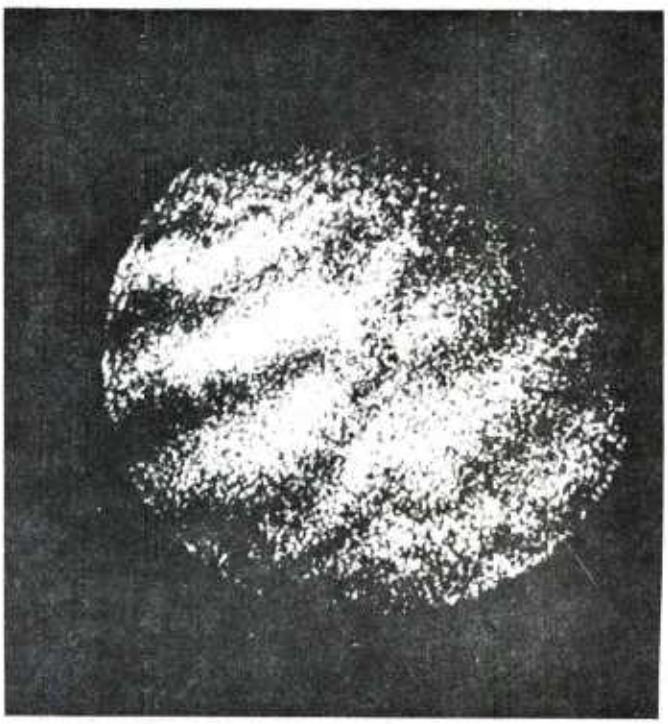

Figure A 8. Test cylinder 65-K-70.

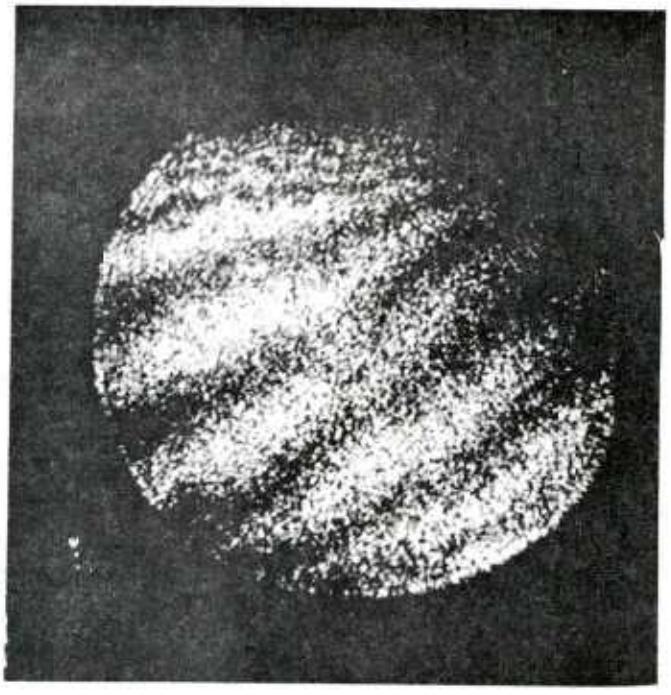

Figure A 9. Test cylinder 69-K-60.

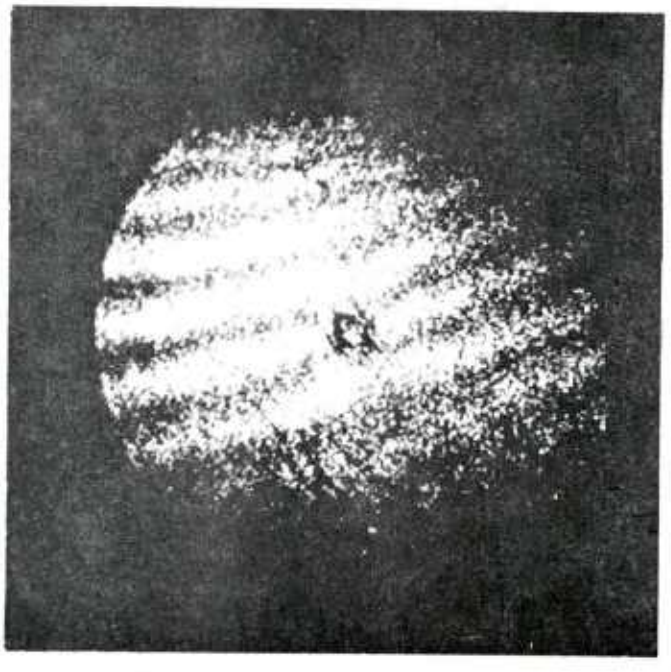

Figure A10. Test cylinder 72-K-45.

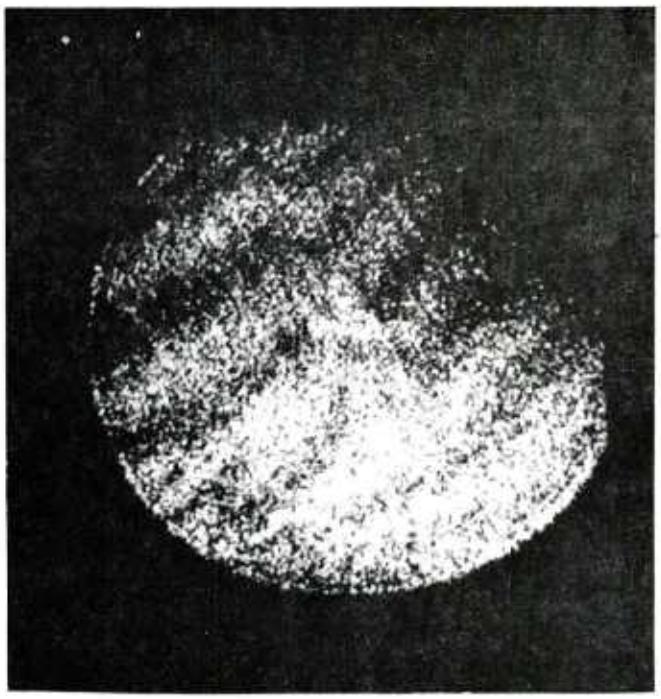

Figure A11. Test cylincer 78-K-60.

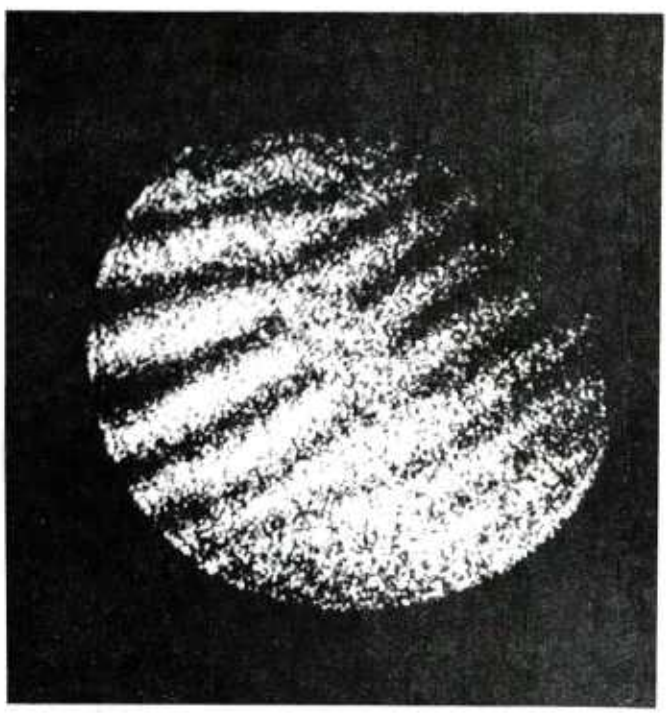

Figure A12. Test cylinder 81-K-45.

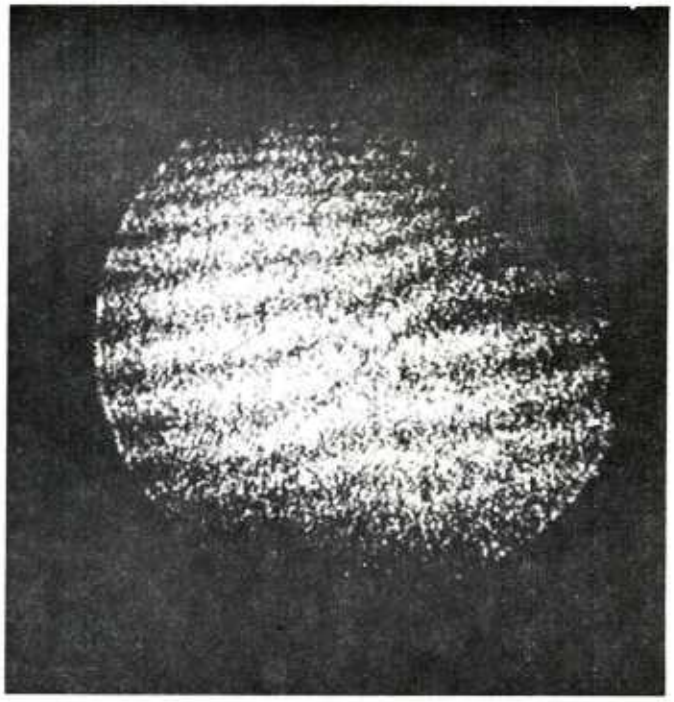

Figure A13. Test cylinder 82-E-70.

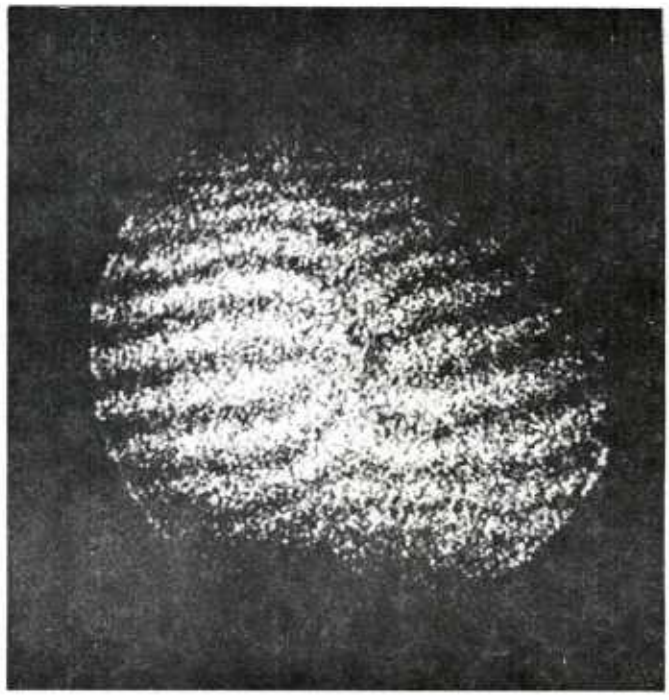

Figure A14. Test cylinder 83-E-70.

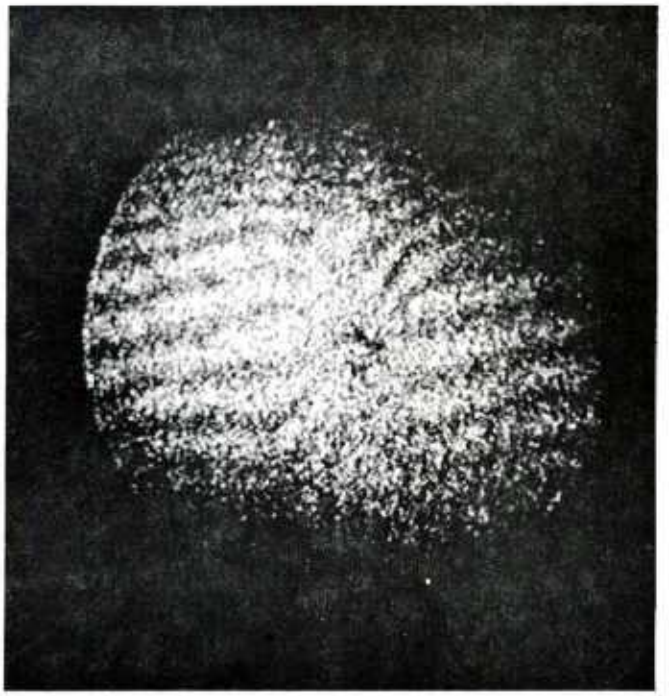

Figure A15. Test cylinder 84-E-70.

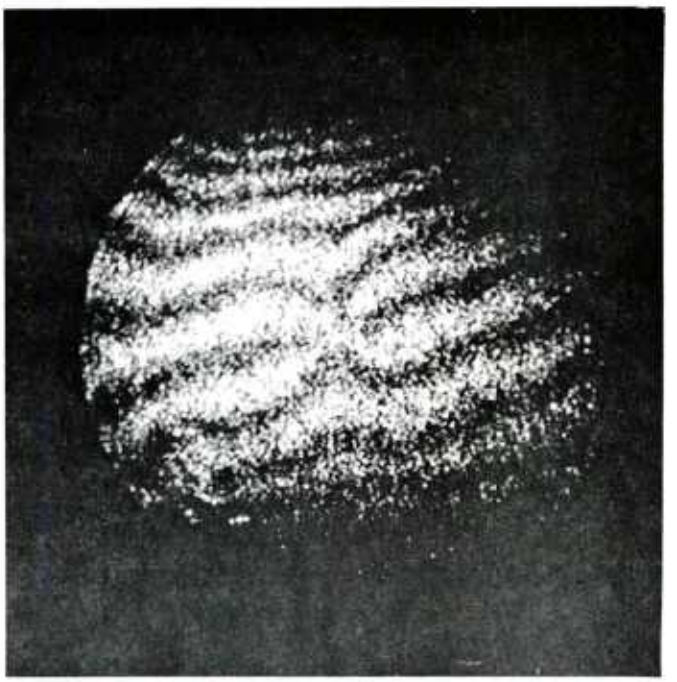

Figure A16. Test cylinder 85-E-60.

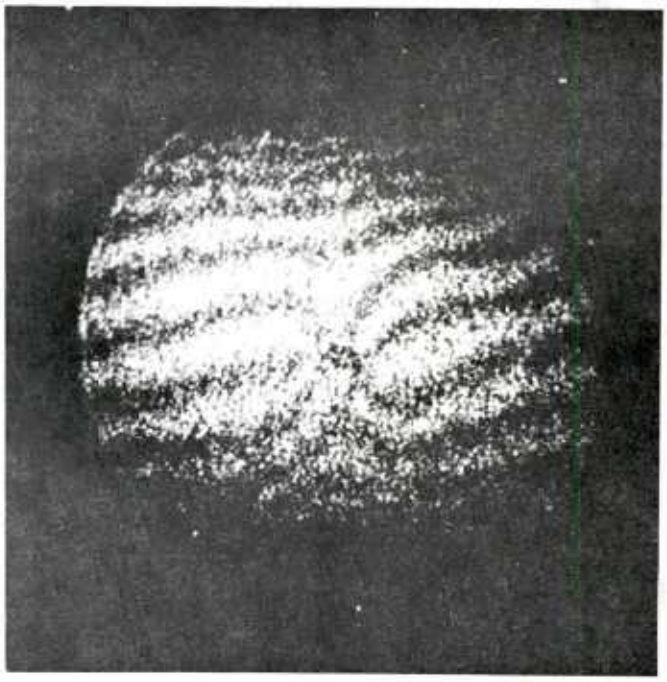

Figure A17. Test cylinder 86-E-60.

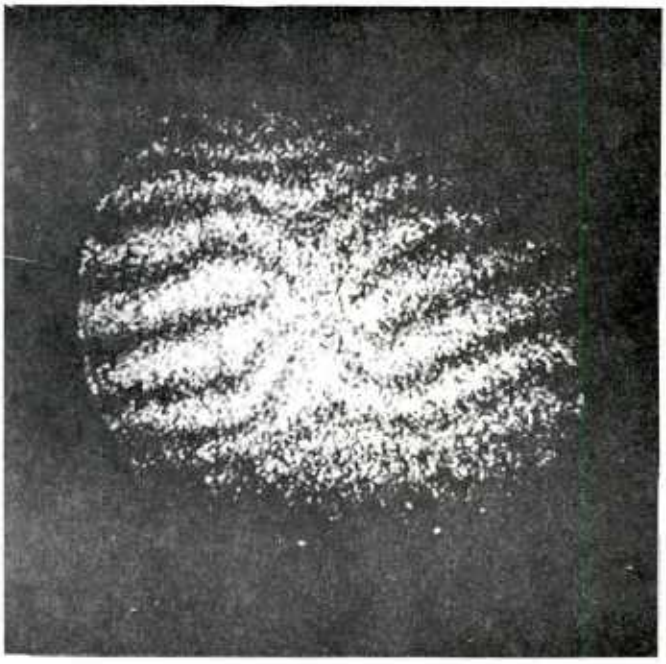

Figure A18. Test cylinder 87-E-60.

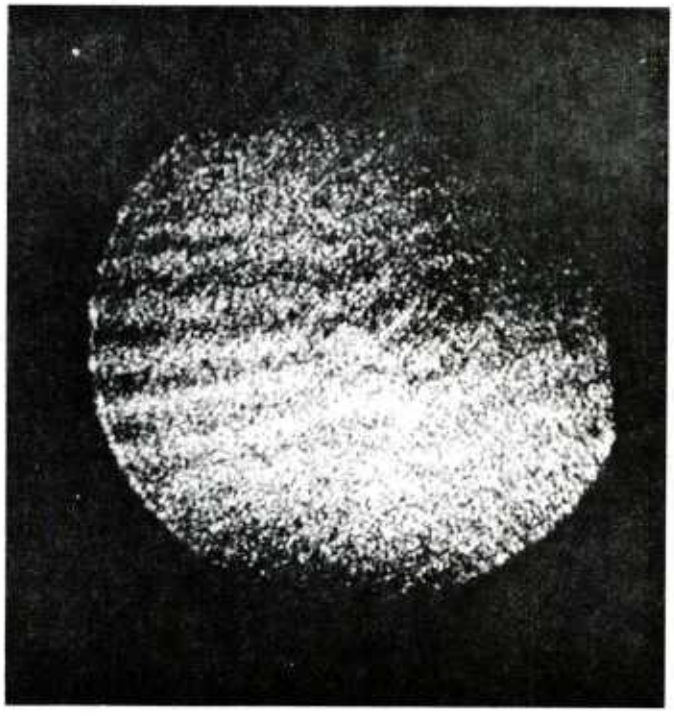

Figure A19. Test cylinder 89-E-45.

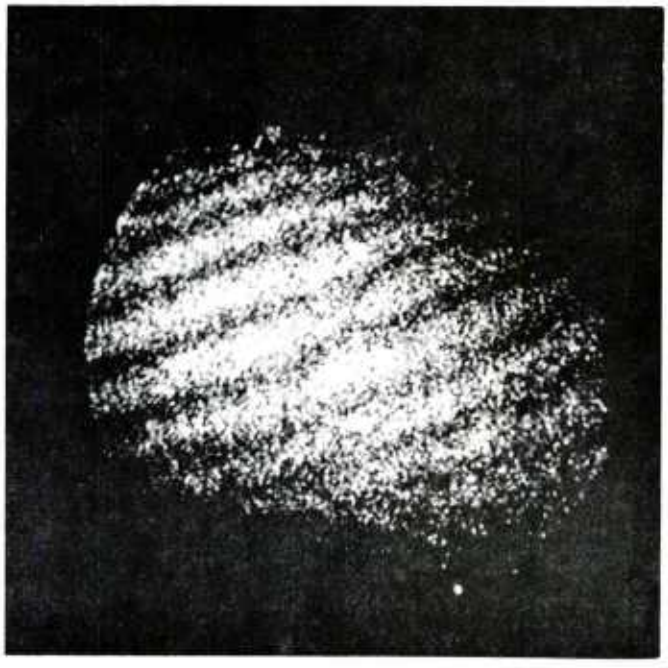

Figure A20. Test cylinder 92-S-70.

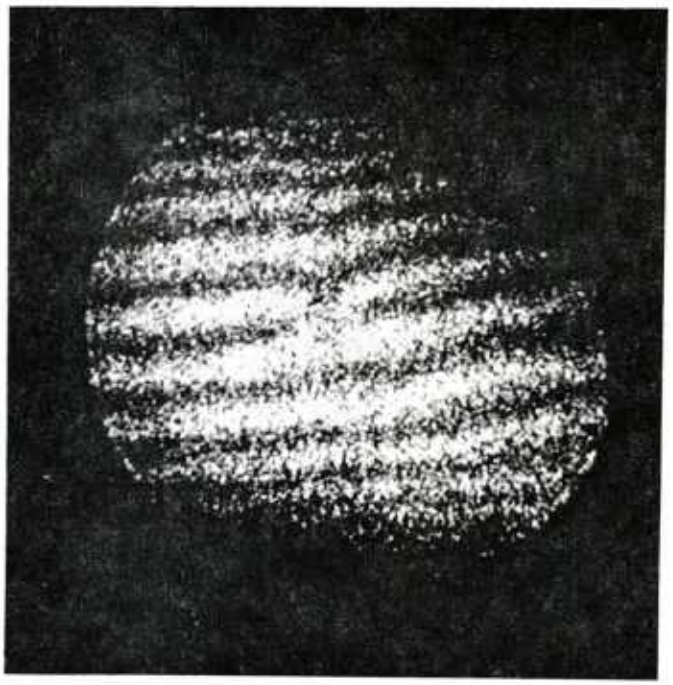

Figure A21. Test cylinder 93-S-70.

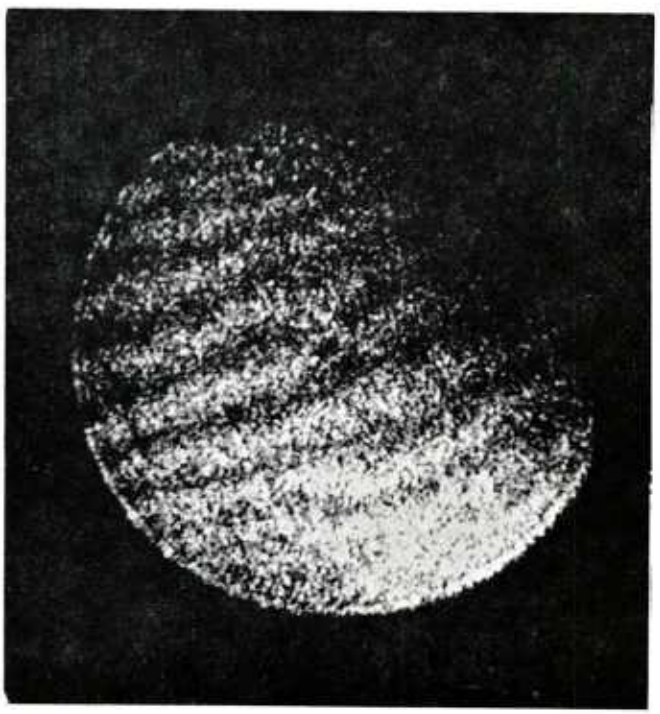

Figure A22. Test cylinder 96-S-60.

APPENDIX B
FULL FIELD RECONSTRUCTION OF HOLOGRAMS

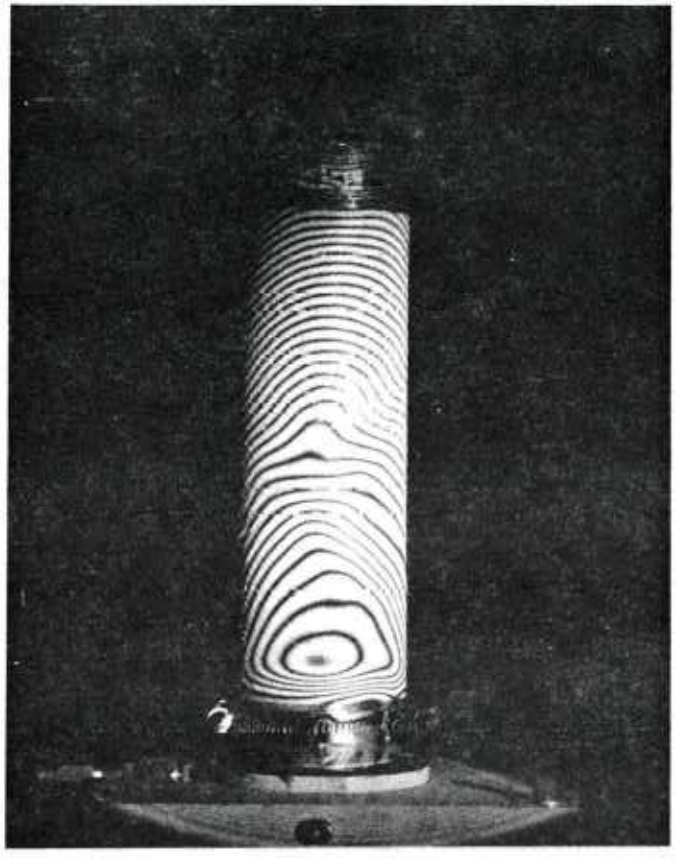

Figure B1. Test cylinder 7-E-45.

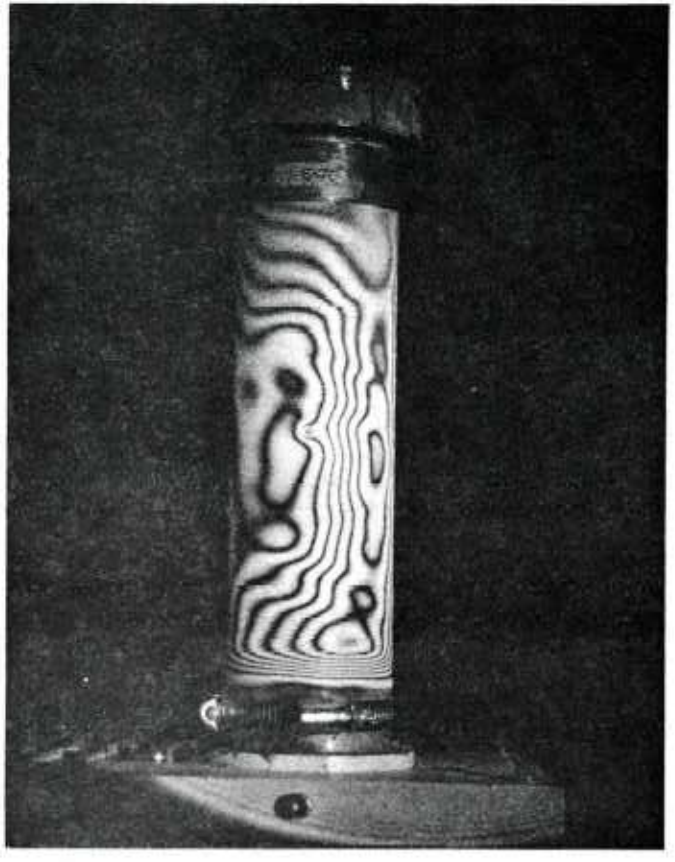

Figure B2. Test cylinder 19-E-70.

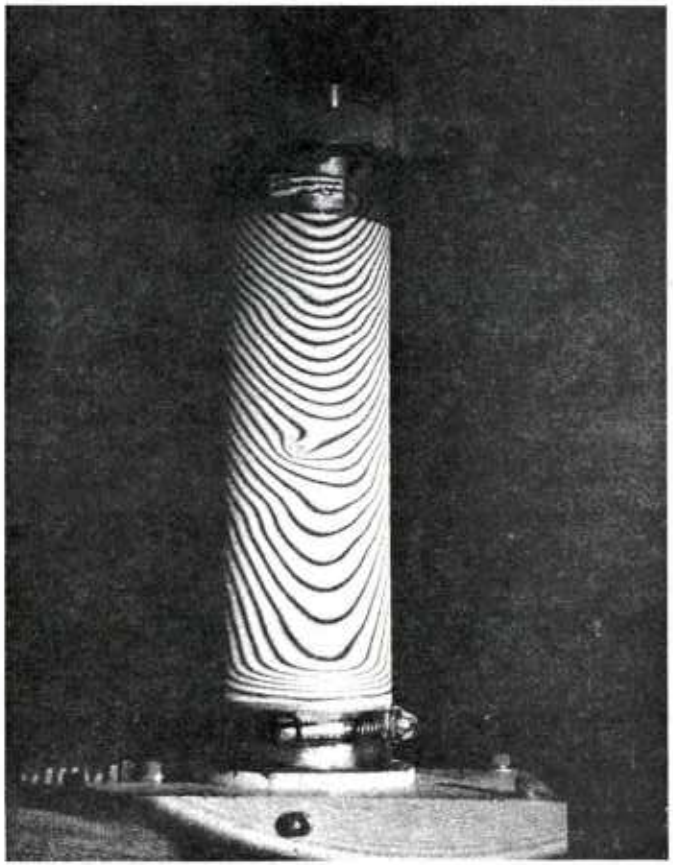

Figure B3. Test cylinder 20-E-70.

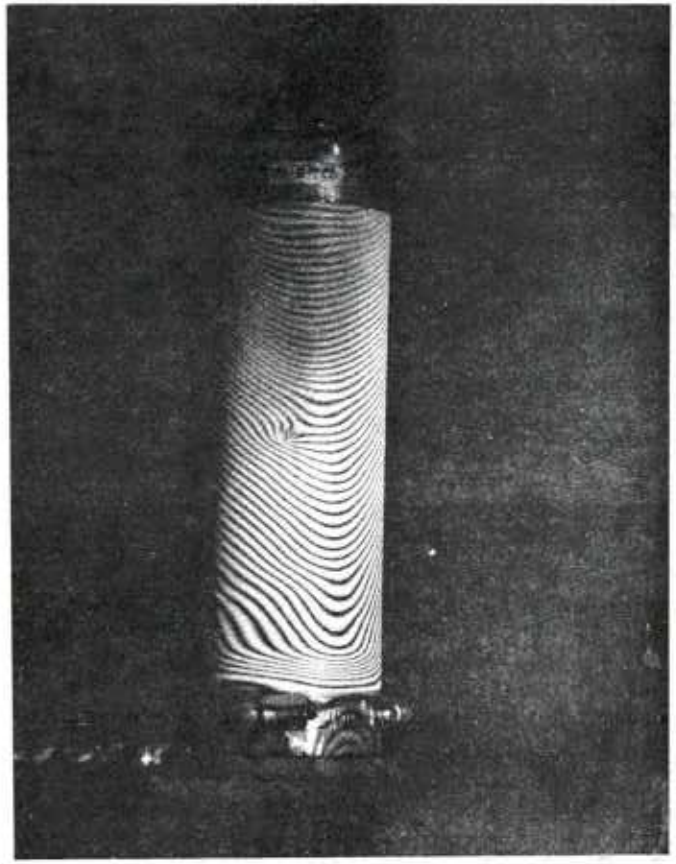

Figure B4. Test cylinder 21-E-70.

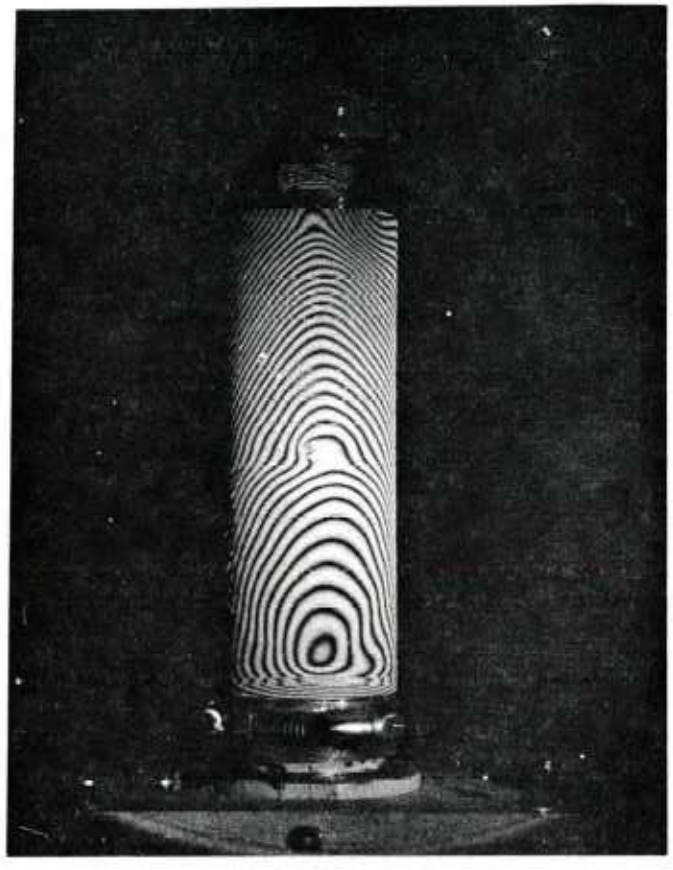

Figure B5. Test cylinder 27-E-45.

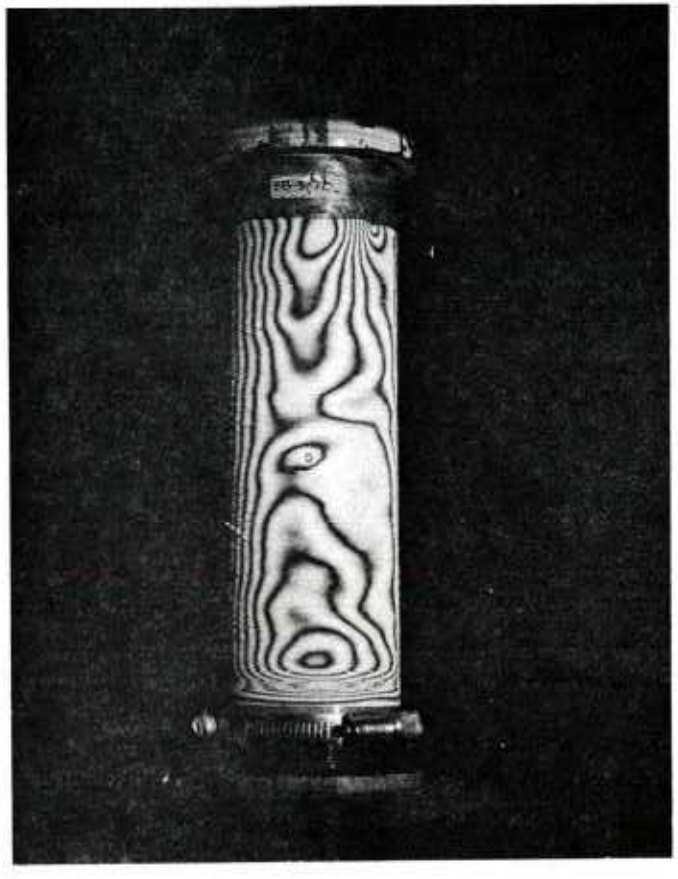

Figure B6. Test cylinder 28-S-70.

Figure B7. Test cylinder 29-S-70.

Figure B8. Test cylinder 30-S-70.

Figure B9. Test cylinder 36-S-45.

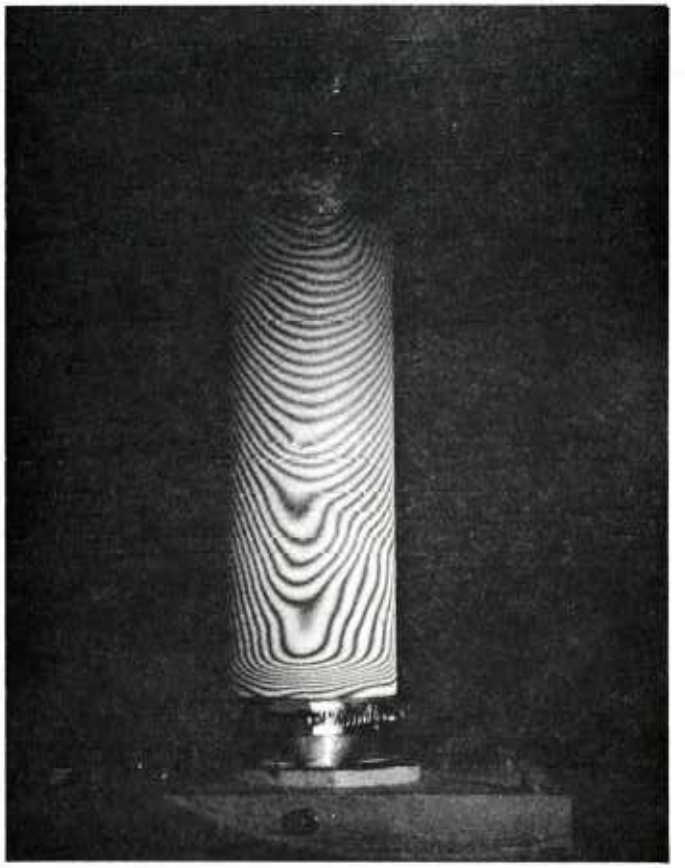

Figure B10. Test cylinder 40-E-60.

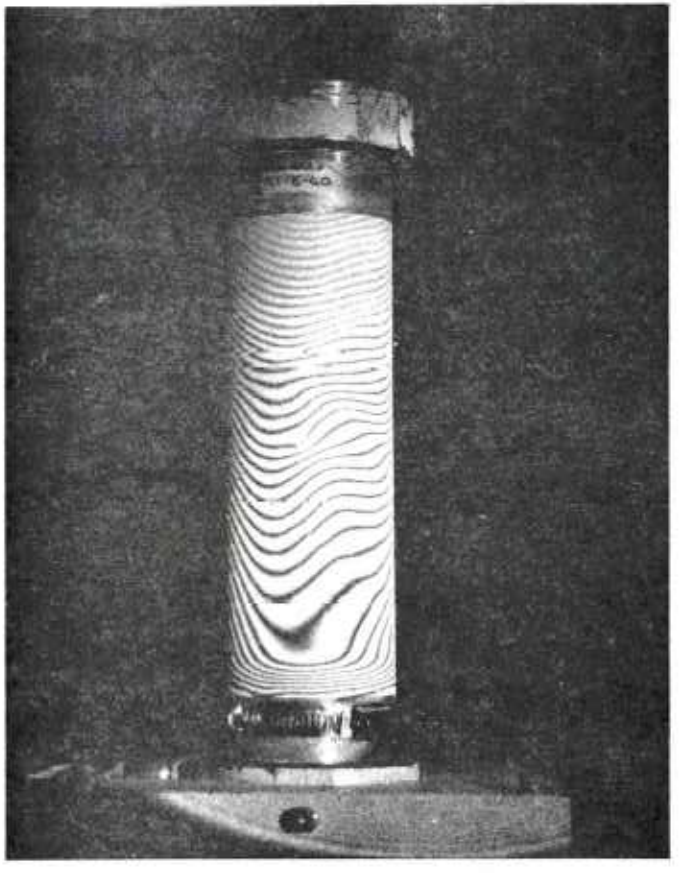

Figure B11. Test cylinder 41-E-60.

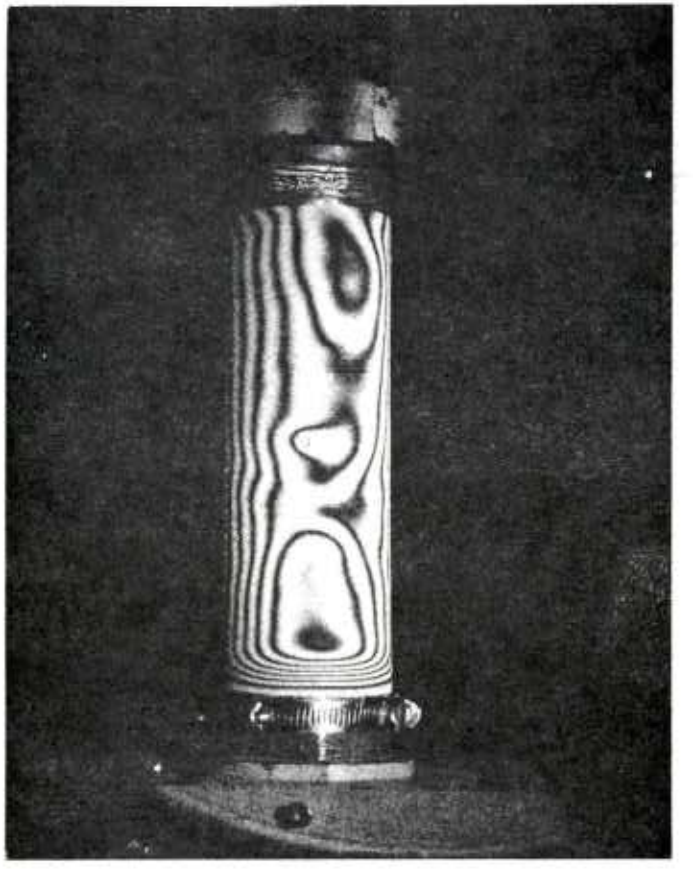

Figure B12. Test cylinder 42-E-60.

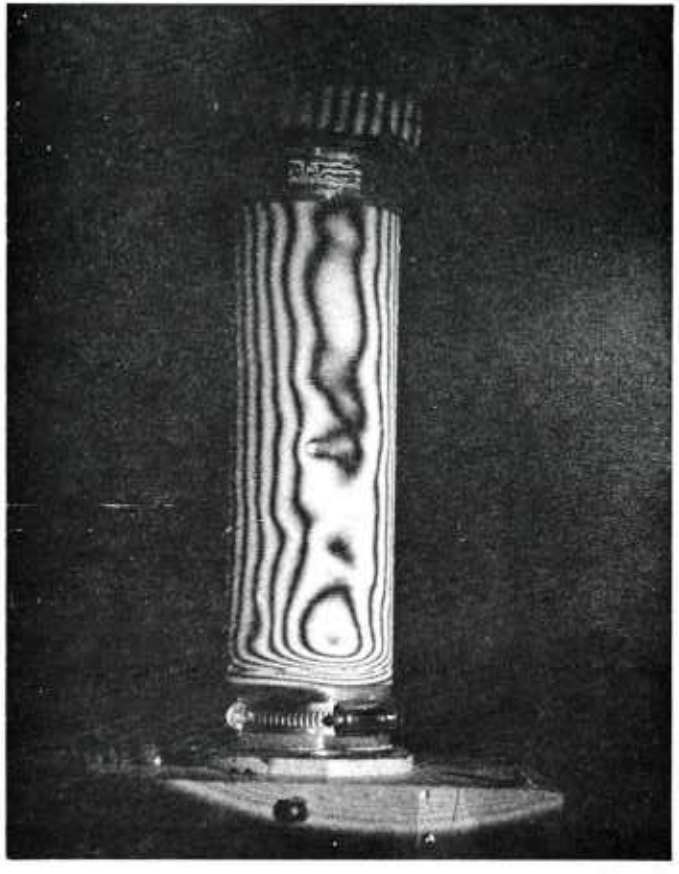

Figure B13. Test cylinder 51-S-60.

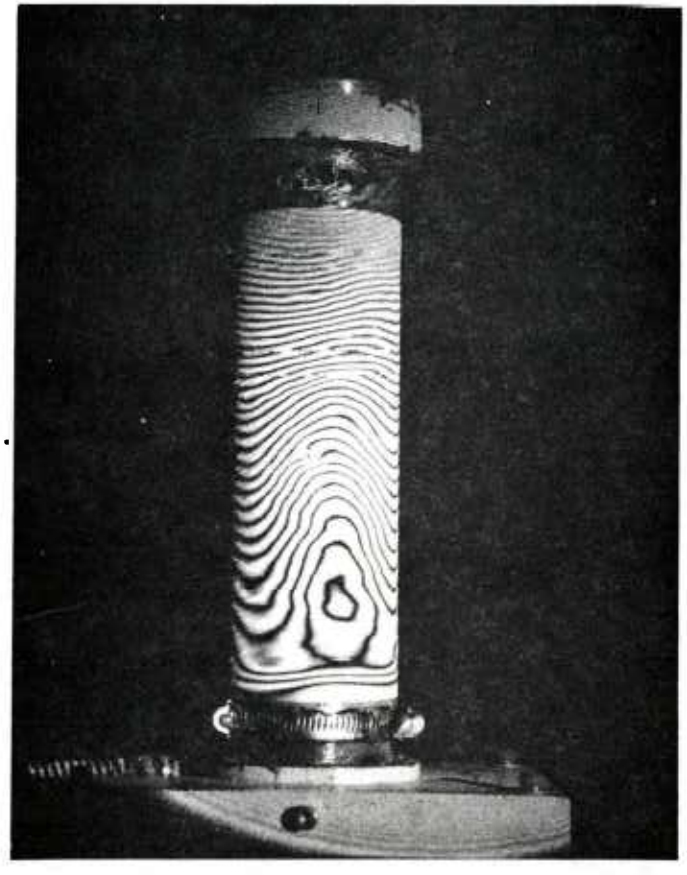

Figure B14. Test cylinder 64-K-70.

Figure B15. Test cylinder 66-K-70.

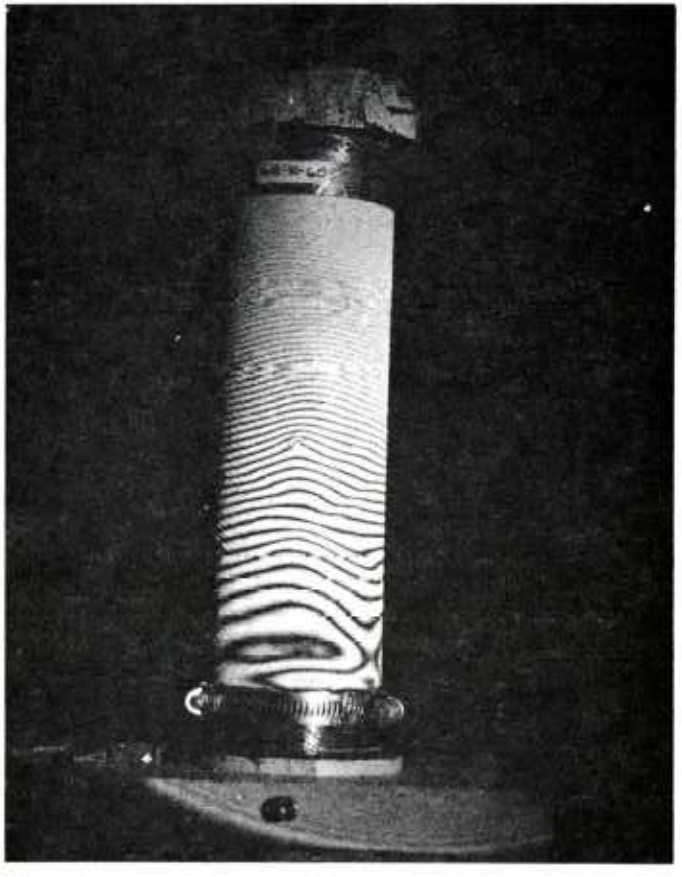

Figure B16. Test cylinder 68-K-60.

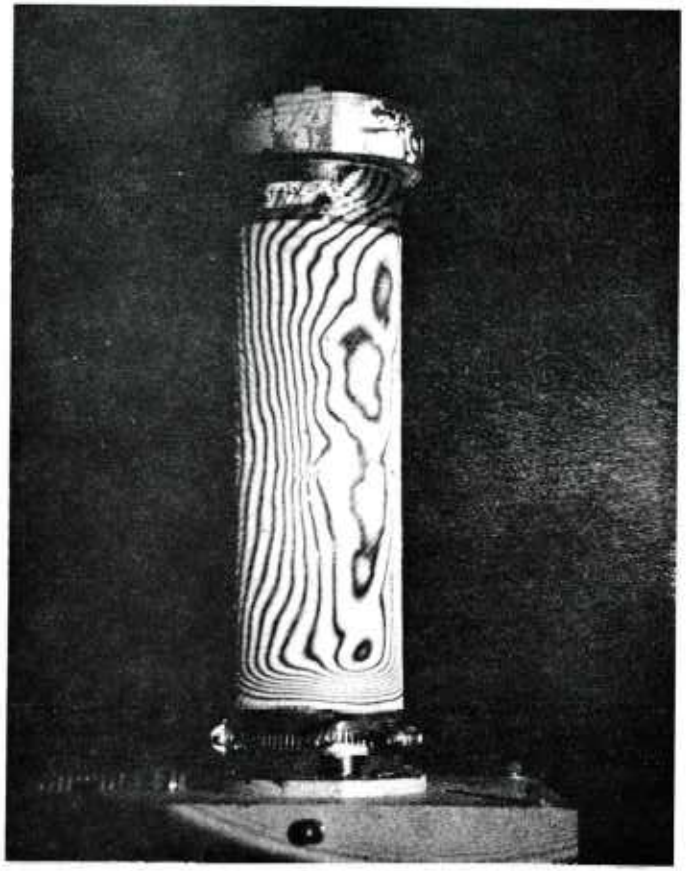

Figure B17. Test cylinder 72-K-45.

Figure B18. Test cylinder 82-E-70.

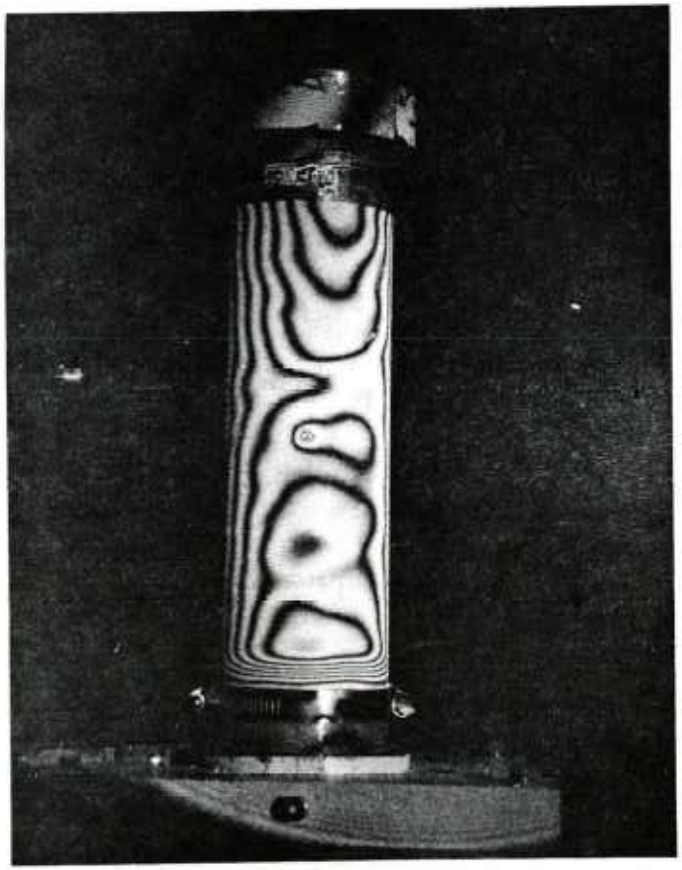

Figure B19. Test cylinder 83-E-70.

Figure B20. Test cylinder 84-E-70.

Figure B21. Test cylinder 86-E-60.

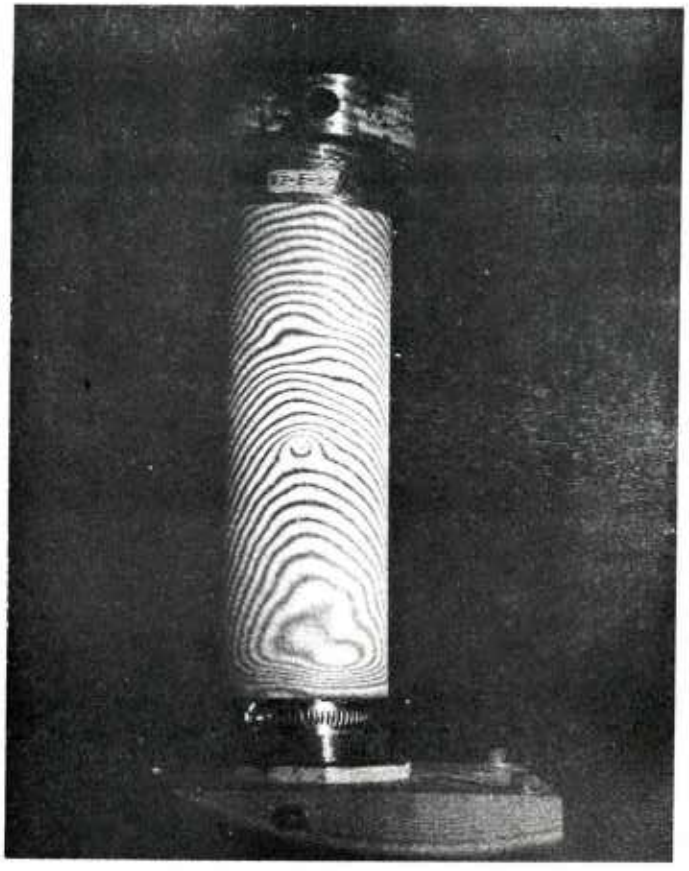

Figure B22. Test cylinder 87-E-60.

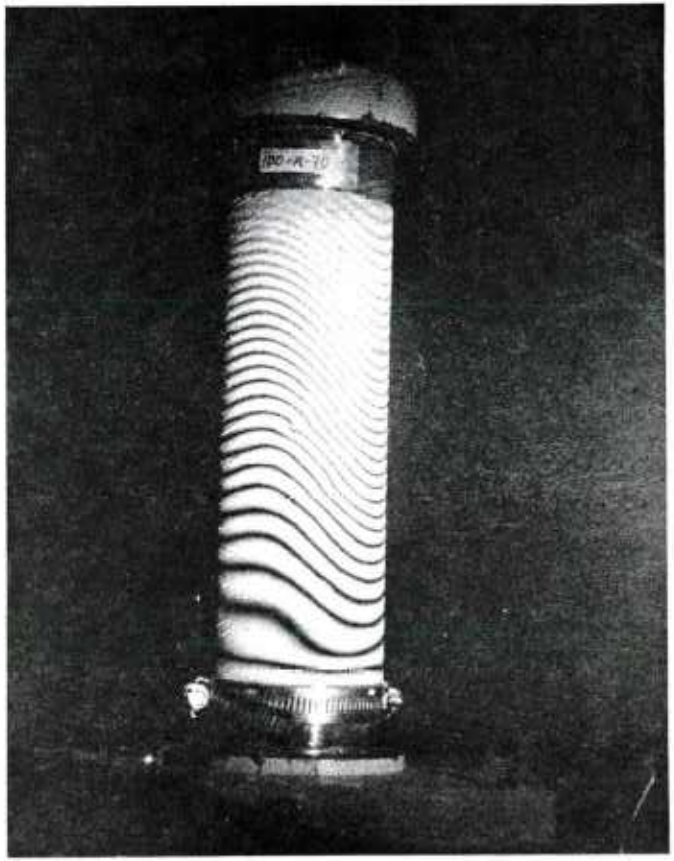

Figure B23. Test cylinder 100-K-70.

Figure B24. Test cylinder 101-K-70.

LIST OF SYMBOLS

SYMBOL	DEFINITION
D	Spacing Between Fringes
f	Distance From Interferogram To Analyzer Screen
K	Magnification Factor
KE	Kinetic Energy
M	Free Fall Mass
m	Fringe Order
n	Constant Contours
p	Distance Aperture is Offset From Focal Point Of Lens
S	Film Scale Factor
U	Inplane Displacement At A Point
U_H	Absolute Displacement Along Horizontal Axis
U_V	Absolute Displacement Along Vertical Axis
$U\chi$	Displacement Along The Direction Parallel To The χ Axis
V	Velocity Of Mass At Impact
Z	Focal Length Of Lens
λ	Wavelength Of Laser Illumination Source
θ	Angle
ν	Optical Geometric Constant
χ	Distance From Central Bright To Center Of Diode

DISTRIBUTION

	No. of Copies
Defense Technical Information Center Cameron Station Alexandria, Virginia 22314	12
Defense Metals Information Center Battelle Memorial Institute 505 King Avenue Columbus, Ohio 43201	1
Commander US Army Foreign Science and Technology Center ATTN: DRXST-SD3 220 Seventh Street, NE Charlottesville, Virginia 22901	1
Office of Chief of Research and Development Department of the Army ATTN: DARD-ARS-P Washington, DC 20301	1
Commander US Army Electronics Command ATTN: DRSEL-PA-P -CT-DT -PP, Mr. Sulkolove Fort Monmouth, New Jersey 07703	1 1 1
Commander US Army Natick Laboratories Kansas Street ATTN: STSNLT-EQR Natick, Massachusetts 01760	1
Commander US Army Mobility Equipment Research and Development Center Fort Belvoir, Virginia 22060	1

DISTRIBUTION (Continued)

	No. of Copies
Director USA Mobility Equipment Research and Development Center Coating and Chemical Laboratory ATTN: STSFB-CL Aberdeen Proving Ground, Maryland 21005	1
Commander Edgewood Arsenal ATTN: SAREA-TS-A Aberdeen Proving Ground, Maryland 21010	1
Commander Picatinny Arsenal ATTN: SARPA-TS-S, Mr. M. Costello Dover, New Jersey 07801	1
Commander Rock Island Arsenal Research and Development ATTN: 9320 Rock Island, Illinois 61201	1
Commander Watervliet Arsenal Watervliet, New York 12189	1
Commander US Army Aviation Systems Command ATTN: DRSAV-EE -MT, Mr. Vollmer St. Louis, Missouri 63166	1 1
Commander US Army Aeronautical Depot Maintenance Center (Mail Stop) Corpus Christi, Texas 78403	1
Commander US Army Test and Evaluation Command ATTN: DRSTE-RA Aberdeen Proving Ground, Marland 21005	1

DISTRIBUTION (Continued)

	No. of Copies
Commander ATTN: STEAP-MT Aberdeen Proving Ground, Maryland 21005	1
Chief Bureau of Naval Weapons Department of the Navy Washington, DC 20390	1
Chief Bureau of Ships Department of the Navy Washington, DC 20315	1
Naval Research Laboratory ATTN: Dr. M.M. Krafft Code 8430 Washington, DC 20375	1
Commander Wright Air Development Division ATTN: ASRC Wright-Patterson AFB, Ohio 45433	1
Director Air Force Materiel Laboratory ATTN: AFML-DO-Library Wright-Patterson AFB, Ohio 45433	1
Director Army Materials and Mechanics Research Center ATTN: DRXMR-PL -MT, Mr. Farrow Watertown, Massachusetts 02172	1 1
Commander White Sands Missile Range ATTN: STEWS-AD-L White Sands Missile Range, New Mexico 88002	1
Deputy Commander US Army Nuclear Agency ATTN: MONA-ZB Fort Bliss, Texas 79916	1

DISTRIBUTION (Continued)

	No. of Copies
Jet Propulsion Laboratory California Institute of Technology ATTN: Library/Acquistions 111-113 4800 Oak Grove Drive Pasadena, California 91103	1
Sandia Laboratories ATTN: Library P.O. Box 969 Livermore, California 94550	1
Commander US Army Air Defense School ATTN: ATSA-CD-MM Fort Bliss, Texas 79916	1
Technical Library Naval Ordnance Station Indian Head, Maryland 20640	1
Commander US Army Materiel Development and Readiness Command ATTN: DRCMT Washington, DC 20315	1
Headquarters SAC/NRI (Stinfo Library) Offutt Air Force Base, Nebraska 68113	1
Department of the Army US Army Research Office ATTN: Information Processing Office P.O. Box 12211 Research Triangle Park, North Carolina 27709	1
Commander US Army Research Office ATTN: DRXRO-PW, Dr. R. Lontz P.O. Box 12211 Research Triangle Park, North Carolina 27709	2
IIT Research Institute ATTN: GACIAC 10 West 35th Street Chicago, Illinois 60616	1

DISTRIBUTION (Continued)

	No. of Copies
Commander Rock Island Arsenal ATTN: SARRI-KLPL-Technical Library Rock Island, Illinois 61201	1
Commander (Code 233) Naval Weapons Center ATTN: Library Division China Lake, California 93555	1
ADTC (DLDSL) Eglin Air Force Base, Florida 32542	1
Commander US Army Materiel Development and Readiness Command ATTN: DRCRD DRCDL 5001 Eisenhower Avenue Alexandria, Virginia 22333	1 1
US Army Research and Standardization Group (Europe) ATTN: DRXSN-E-RX, Dr.. Alfred K. Nodoluha Box 65 FPO New York 09510	2
Headquarters Department of the Army Office of the DCS for Research Development and Acquisition Room 3A474, The Pentagon ATTN: DAMA-ARZ Washington, DC 20310	2
US Army Materiel Systems Analysis Activity ATTN: DRXSY-MP Aberdeen Proving Ground, Maryland 21005	1
University of California Los Alamos Scientific Laboratory ATTN: Reports Library P.O. Box 1663 Los Alamos, New Mexico 87545	1

DISTRIBUTION (Concluded)

	No. of Copies
Director Defense Advanced Research Projects Agency 1400 Wilson Boulevard Arlington, Virginia 22209	1
DRSMI-IYB	1
DRSMI-LP, Mr. Voigt	1
DRSMI-R, Dr. Kobler	1
-RE	1
-REM	1
-REP	1
-RES	1
-RET	3
-RL, Mr. Lewis	1
-RLA, Mr. Pettey	1
-RLA, Mr. Vandiver	50
-RPR	3
-RPT (Reference Copy)	1
-RPT (Record Copy)	1

☆ U.S. GOVERNMENT PRINTING OFFICE: 1980—640-287/749